Doctoral Dissertations   Graduate School

Spring 5-25-2019

Fundamental Understanding of Microstructural Properties of Electrolyte System for NOx Exhaust Gas Sensing

Khawlah Kharashi
Louisiana Tech University

Follow this and additional works at: https://digitalcommons.latech.edu/dissertations

Recommended Citation

Kharashi, Khawlah, "" (2019). *Dissertation*. 42.
https://digitalcommons.latech.edu/dissertations/42

This Dissertation is brought to you for free and open access by the Graduate School at Louisiana Tech Digital Commons. It has been accepted for inclusion in Doctoral Dissertations by an authorized administrator of Louisiana Tech Digital Commons. For more information, please contact digitalcommons@latech.edu.

FUNDAMENTAL UNDERSTANDING OF MICROSTRUCTURAL

PROPERTIES OF ELECTROLYTE SYSTEM FOR

NO$_X$ EXHAUST GAS SENSING

by

Khawlah Kharashi,

A Thesis Presented in Partial Fulfillment
of the Requirements of the Degree
Doctor of Philosophy

COLLEGE OF ENGINEERING AND SCIENCE
LOUISIANA TECH UNIVERSITY

February 2018

LOUISIANA TECH UNIVERSITY

THE GRADUATE SCHOOL

_____

Date

We hereby recommend that the thesis prepared under our supervision by

Khawlah Kharashi, **PhD.**

entitled   **Fundamental Understanding Of Microstructural Properties Of**

Nox Exhaust Gas Sensing

_____

be accepted in partial fulfillment of the requirements for the Degree of

Master of Science inMolecular Science and Nanotechnology)

_____

Supervisor of Thesis Research

_____

Head of Department

Science

Department

Recommendation concurred in:

_____

_____

Advisory Committee

_____

_____

Approved: **Approve**d:

_____   _____

Director of Graduate Studies   Dean of the Graduate School

_____

Dean of the College

ABSTRACT

The nitrogen oxides (NO_x) sensors available on the market are unable to detect minute concentrations of NO_x (<10 ppm) and, as a result, they are unable to meet the new US standards, i.e. Tier 3 standards for the period of 2017-2025. As per these standards sensors should be highly sensitive and capable of determining NO_x on the order of single parts per million. As compared to gasoline engines, diesel engines have greater efficiency per unit quantity of fuel consumed, but they emit more smog causing NO_x.

The three-way catalyst systems in modern diesel engines are ineffective in chemically reducing nitrogen oxides in the presence of excess air. Even though a number of NOx abatement systems have been developed over the years, the after-treatment systems in vehicles require a highly sensitive NO_x sensor capable of monitoring low concentrations of NO_x in the exhaust gases. The solid state electrochemical sensors, having porous yttria-stabilized zirconia (YSZ), along with dense electrodes, exhibit enhanced NO_x sensitivity. Porous electrolytes support gas diffusion, while the dense electrodes limit heterogeneous catalysis reactions that interfere with accurate sensing of NO_x.

The primary aim of this study was to investigate porous electrolytes composed of fully-stabilized YSZ (FSZ) and partially-stabilized YSZ (PSZ) incorporated with α-alumina (Al_2O_3) as well as gold (Au) wires as electrodes. The impedancemetric study of porous PSZ based sensors added with different weight percentages (2, 3.8, 5 and 10) of Al_2O_3 was conducted at varying operating conditions. The addition of 2 wt%

iii

Al_2O_3 to PSZ resulted in an increase in the NO_x sensor impedance and grain boundary conductivity. However, above 2 wt% Al_2O_3 in the PSZ, the resistance of the electrolyte bulk and grain boundaries was increased. The PSZ based sensor with 2 wt% Al_2O_3 resulted in greater sensitivity at concentrations as low as 5 ppm NO_x.

Composite electrolytes consisting of PSZ, FSZ, and PSZ–FSZ were studied by using impedance spectroscopy for the electrochemical responses under dry and humidified gas conditions. The response of 50 PSZ–50 FSZ based sensors indicated contribution of PSZ to lower water cross-sensitivity, while FSZ promoted NO_x sensitivity. The microstructure of each electrolyte influenced sensor sensitivity, but there was no impact on water cross-sensitivity.

APPROVAL FOR SCHOLARLY DISSEMINATION

The author grants to the Prescott Memorial Library of Louisiana Tech University the right to reproduce, by appropriate methods, upon request, any or all portions of this Thesis. It is understood that "proper request" consists of the agreement, on the part of the requesting party, that said reproduction is for his personal use and that subsequent reproduction will not occur without written approval of the author of this Thesis. Further, any portions of the Thesis used in books, papers, and other works must be appropriately referenced to this Thesis.

Finally, the author of this Thesis reserves the right to publish freely, in the literature, at any time, any or all portions of this Thesis.

Author _____

Date _____

DEDICATION

I would like to dedicate my thesis to my beloved family.

TABLE OF CONTENTS

LIST OF FIGURES

LIST OF TABLES

ACKNOWLEDGMENTS

CHAPTER 1.

INTRODUCTION

1.1 Overview

This dissertation encompasses a comprehensive yet concise review of research findings on the microstructural properties of the Nitrogen oxide (NO) and nitrogen dioxide (NO_2) which together are called (NO_x) sensor electrolytes. An effort has been made to relate the impact of microstructural properties of different electrolytes on the performance of their respective NO_x sensors. At present, the NO_x sensors available on the market are unable to detect minute concentrations of NO_x (<10 ppm) and, as a result, they are unable to meet the future regulations pertaining to automobile exhaust emissions.

In current vehicles, a NO_x sensor is located in the diesel exhaust pipe after the emissions abatement hardware. The primary purpose is to monitor the performance of the NO_x abatement system by analyzing the exhaust gases passing through the tailpipe. The new US standards, i.e. Tier 3 standards for the period of 2017-2025, require that the sensor should be highly sensitive and capable of determining NO_x on the order of single parts per million.

1.2 Motivation

Diesel emissions contain nitrogen oxide gases and other toxic particles, the smallest of which contribute to lung and heart disease. Increases in airborne fine particulate matter increases the risk for myocardial infarctions, strokes and heart

failure. Therefore, detection and regulation of NO_x in diesel engine is of key importance and is an important area of research in order to limit the amount of the NO_x in the environment. As compared to gasoline engines, the diesel engines have greater efficiency per unit quantity of fuel consumed, but they emit more NO_x causing smog. In diesel engines, the three-way catalyst systems are ineffective in chemically reducing nitrogen oxides in the presence of excess air. A number of NO_x abatement systems have been developed ranging from engine modifications e.g., (changes in injector location, fuel pressure) to NO_x control hardware systems i.e., (selective catalytic reduction, and lean NO_x traps) fitted in the diesel exhaust pipe. Overall, diesel after – treatment systems in vehicles require a highly sensitive NO_x sensor capable of monitoring low concentrations of NO_x in the exhaust gases.

Porous electrolyte based NOx sensors enhanced NO_x sensitivity which typically incorporate electrodes with a dense microstructure. The porous electrolyte supports gas diffusion, while the dense electrodes limit heterogeneous catalysis reactions that interfere with accurately sensing nitrogen oxide (NO) and nitrogen dioxide (NO_2). The goal of these studies has largely concentrated on porous electrolytes composed of fully-stabilized yttria-doped zirconia (YSZ) due to the high ionic conductivity of the material that is known to promote NO_x sensitivity from diesel engines and lower cross-sensitivity to water by using composite electrolyte NO_x sensors with a porous microstructure.

In this thesis study, fully-stabilized yttria-doped zirconia (FSZ, 4.7 mol.% $Y_2O_3–ZrO_2$), Partially-stabilized yttria-doped zirconia (PSZ, 4.7 mol.% $Y_2O_3–ZrO_2$), and α- Al_2O_3. as well as twine Au wires electrodes were studied. Compared to the conventional sensors (such as potentiometric and amperometric), the NO_x sensors utilizing YSZ-based electrolytes have been found to be effective in detecting nitrogen

oxides at very low concentrations. However, the Impedancemetric study of gas sensors is still under development because of a number of challenges such as cross sensitivity to oxygen and water vapors present in the exhaust gases.

1.3   Dissertation Organization

The organization of this dissertation is given as follows:

- Chapter 2 provides a detailed overview of NO_x emissions and the related regulations set by the major economies of the world. In addition, the different types of exhaust gas sensors are also discussed.

- Chapter 3 encompasses the basic concepts in electrochemical impedance spectroscopy.

- Chapter 4 provides the details of Al_2O_3 effect in porous YSZ-based electrolytes for NO_x sensing applications.

- Chapter 5 describes the research study on the management of H_2O cross-sensitivity of NO_x sensors by using composite electrolytes.

- Chapter 6 details the application of the enhanced composite electrolytes.

- Chapter 7 summarizes the results and gives a discussion regarding future work and conclusions.

CHAPTER 2.

BACKGROUND

In this chapter, Section 2.1 discusses the improvement in diesel engine technology. Section 2.2 discusses the air quality programs in the United States and Europe that focus on reduced NO_x gases followed by Section 2.3 which presents a compact discussion about different NO_x Exhaust gas sensors. The last section of this chapter discusses the chemical structure of the zirconia electrolytes NO_x sensors along with the microstructural and electrical properties of zirconia.

2.1   Advancement in Diesel Engine Technology

Diesel engines offer greater torque and higher efficiency in comparison to gasoline engines. However, the nitric oxide (NO_x) emissions are significantly greater. This is a problem because NO_x emissions contributor to poor air quality that negatively impact the environment and human health. Substantial efforts have focused on lowering NO_x emissions as diesel engine technology progresses. Key strategies for lowering NO_x emissions include lean NO_x traps (LNT) and selective catalytic reduction (SCR). Lean NO_x traps are the most common exhaust gas after-treatment system used with diesel engines.

In this system, while the engine runs under lean conditions, the trap converts nitric oxide into nitrogen and water. The advantages of LNT technology include high NO_x removal activity, which helps to address cold-start problems, while also being cost-effective. The first few minutes of engine operation is considered cold start, as

the engine block and coolant temperatures are low resulting in incomplete combustion. Cold start is a problem because it results in significantly higher emissions, in comparison to an engining operate at higher temperatures. LNT technology enables immediate conversion of NO_x that is generated from the engine to N_2 and water in order to control the harmful gases that cause pollutions and improve air quality. However, the burst of fuel needed to regenerate the trap is a large disadvantage as engine fuel efficiency is reduced.

Selective catalytic reduction (SCR) is costly in comparison to LNTs; however, the emissions are significantly lower with this exhaust after-treatment system. A selective catalytic reduction system uses a metallic or ceramic wash-coated catalyzed substrate and a chemical reductant to convert nitrogen oxides to molecular nitrogen and oxygen in the exhaust streams of the diesel engines. Using an aqueous urea solution, such as AdBlue, is usually the chosen reductant for the SCR system. However, there is a problem with this system, which is the majority of the NO_x emissions occur during cold-start. SCR systems do not work well at temperatures below 150°C, which means a good amount of NO_x is not treated during cold-start conditions. Although this is an issue, the SCR systems are still preferred because this technology is significantly less expensive than LNT systems along with the higher NO_x reduction with lower NO_x concentrations. Moreover, it does not require modification to the combustion unit. Figure 2-1 shows the SCR system in 2017 diesel trucks.
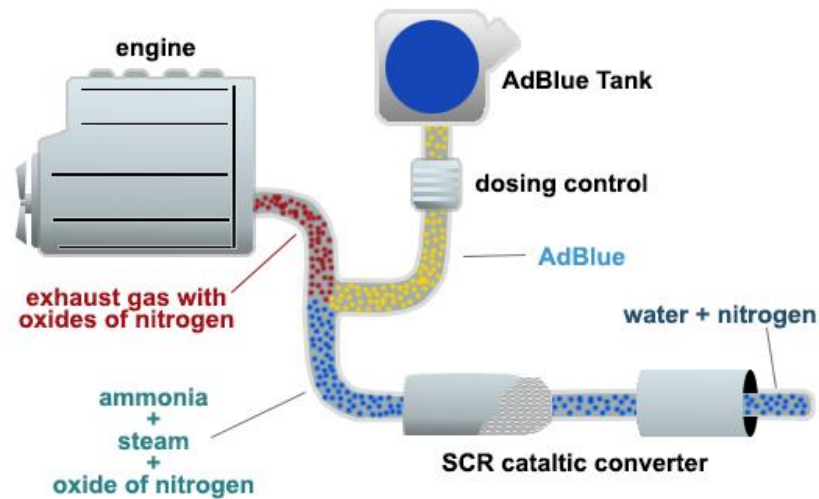
Figure 2-1: The SCR System in 2017 Diesel Trucks [1].

NO$_x$ sensors play a crucial role in monitoring and controlling diesel engine operation and exhaust after-treatment systems. As advancements in diesel engine technology results in lower emissions, it is important for NO$_x$ sensors to be capable of measuring lower diesel emissions with high sensitivity, selectivity and accuracy.

2.2   Automotive Emissions Standards

Diesel vehicles require NO$_x$ sensors that monitor exhaust gases according to governmental regulations for automotive emissions. Nowadays, limiting the NO and NO$_2$ exhaust species become the most challenging because these gases are considered very dangerous pollutants to the air. The Environmental Protection Agency (EPA) in the US and regulatory agencies in Europe and other countries have issued stringent standards for heavy duty highway diesel vehicles to limit NO$_x$ emissions.

There are many forms of nitrogen oxides ranging from nitric oxide to dinitrogen pentoxide. There are a total of seven forms which are shown in **Table 2-1**. These oxides could occur naturally and can take different forms through other natural processes such as lightning, forest fires, and emissions [2].

Table 2-1: Different oxides of Nitrogen [2].

Formula	Name
NO	Nitric oxide
NO_2	Nitrogen dioxide
N_2O	Nitrous oxide
NO_3	Nitrogen trioxide
N_2O_4	Nitrogen tetroxide
N_2O_3	Dinitrogen trioxide
N_2O_5	Dinitrogen pentoxide

Among the different nitrogen oxides, only NO and NO_2 are found naturally and they virtually constitute all nitrogen oxide emissions. Anthropogenic emissions of these oxides are predominantly related to combustion processes. These processes include vehicle emissions, gas turbines, boilers, and industrial burners [3, 4]. The emissions of NO_x are particularly under observation because of their contribution to atmospheric pollution. Nitrogen oxide combines with ozone to form nitrogen dioxide. The nitrogen dioxide is a brown gas which is responsible for smog formation and adverse effects on health such as respiratory problems. Moreover, the atmospheric NO_2 also combines with rainwater and causes acid rain [2].

The general photochemical reaction leading to the formation of nitrogen dioxide is given in **Eq. 2-1** [5]:

$$NO + O_3 \overset{h\nu}{\leftrightarrow} NO_2 + O_2 \qquad \textbf{Eq. 2-1}$$

All over the world, there are different regulations which determine the NO_x emissions in a particular region. The major economies of the world such as the United States and Europe have different NO_x emission standards. These standards cannot be compared directly due to difference in the testing parameters. However, these standards tend to converge to even lower values of emissions over time. These two standards are shown in **Figure 2-2.**
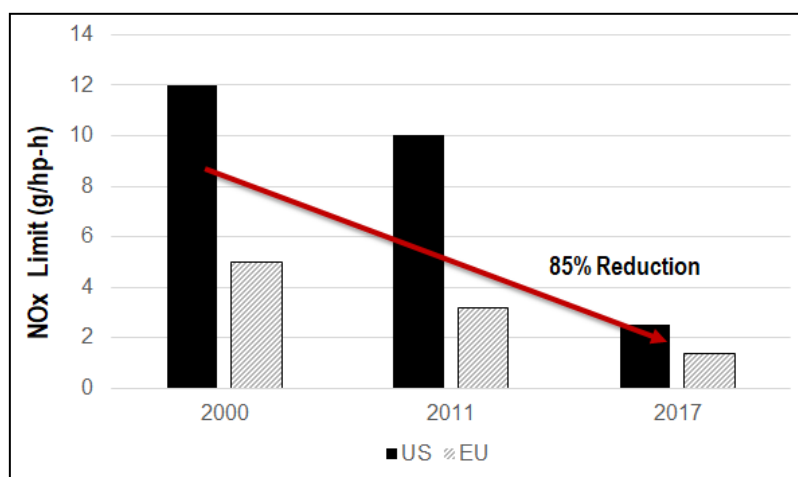
Figure 2-2: US and EU have different NO_x emission standards for heavy duty diesel engines.

The US EPA Tier 2 standards were implemented in 2004. They are now phased out and have been replaced by Tier 3 standards for the period of 2017-2025 [7]. Therefore, to meet strict standards for diesel vehicles based on the data in **Figure 2-2**, researchers must focus on creating more advanced NO_x sensors. Such sensors need to monitor the exhaust and regulate diesel engine operation within the required emissions standards. These advanced NO_x sensors should have the following capabilities:

- Stability within ±1 ppm accuracy
- Sensitivity to low gas concentrations (less than 10 ppm NO_x)

- Better selectivity to NO_x in the presence of other gases such as oxygen and water vapor

- Smooth and stable operation for a long period of time (such as 100,000 hours)

- Repeatable and reproducible output signal

- Simplicity in design and control

- Robustness in design (sensor material resistant to chemical degradation, changes in morphology, crystallographic changes, and so on)

- Ability to work effectively in high temperature ranges (500 to 900°C)

- Simple and low-price application process that can be used on commercial scale for mass production

2.3   Operating Principles of NO_x Exhaust Gas Sensors

The most common type of NO_x sensor inside the diesel vehicle exhaust system is the amperometric sensor. This type of sensor typically utilizes a dense zirconia electrolyte, along with porous platinum electrodes. An operational scheme of amperometric sensor is shown in **Figure 2-3**. The sensor utilizes multiple electrochemical cells in adjacent chambers [6]. The purpose of the first chamber is to remove any excess quantity of oxygen present in the exhaust gases, whereas the purpose of the second chamber is to detect NO_x in the exhaust gases. The mechanism of detection, which is based on the diffusion of gases through multi-chambers provided with small orifices at the entry, results in slower operation of the sensor. On the other hand, this sensor is able to detect lower concentrations of NO_x compared to the other commercially available sensors [7, 8].
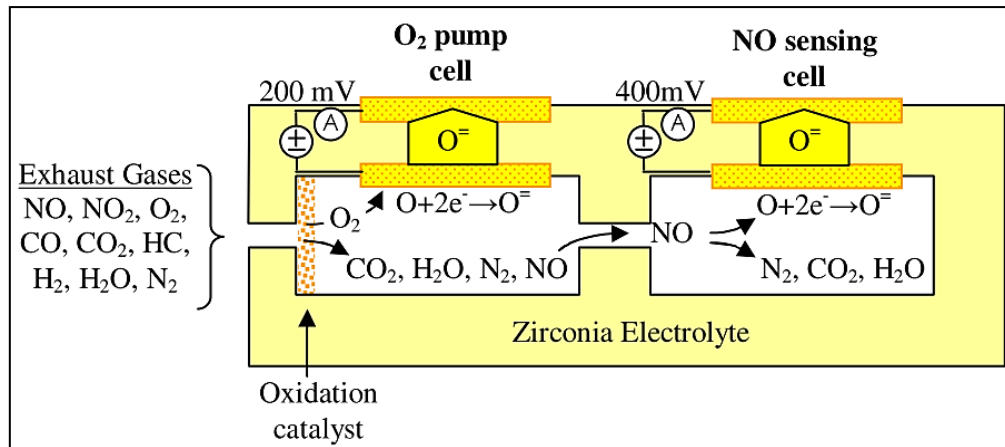
Figure 2-3: Operational Scheme of Amperometric NOx sensor [9].

The amperometric sensor is designed to minimize interference from O_2 and provide total NO_x detection. Current sensors are capable of detecting NO_x at concentrations around 100 ppm and greater. In terms of the associated electronics and sensor design, when compared with other sensors, the amperometric sensors possess complex characteristics that add cost of the device. Advancement of diesel engine technology is resulting in lower NO_x emissions and the new regulatory standards require monitoring capabilities of sensors for NO_x at levels of 10 ppm and lower. Considering this, there is a concern that current amperometric NO_x sensors will not be effective. Therefore, alternative NO_x sensing method are being researched and are discussed below.

2.4 Potentiometric Sensors

Potentiometric (i.e. mixed potential) NO_x sensors have been considered as an alternative to amperometric NO_x sensors. YSZ is a common electrolyte of potentiometric NO_x sensors. Numerous materials have been used for the sensing electrode, such as precious metals, spinel type oxides, and perovskites. The electrolyte is embedded between two electrodes (the reference electrode and the sensing electrode). In this type of sensor, the sensing response is determined by measuring the

potential difference between the sensing and counter electrodes of the electrochemical cell. Both oxidation and reduction reactions occur simultaneously on a single electrode. This results in a non-Nerstian, potentiometric sensor. Numerous electrochemical reactions can occur at the same conductive service.

The potentiometric NO_x sensors possess inherently simple cell design (**Figure 2-4**) and can be fabricated at a low cost compared to the amperometric sensors. Because of these attractive features, they have been extensively studied in the last decade [10, 11]. However, potentiometric NO_x sensors are cross-sensitive to the O_2, CO, and hydrocarbons. Moreover, additional measures are needed to enable total NO_x sensing. Because the sensitivity sign of NO_2 is relatively opposite to NO in mixed potential sensor, it is difficult to monitor the total NO_x sensing.
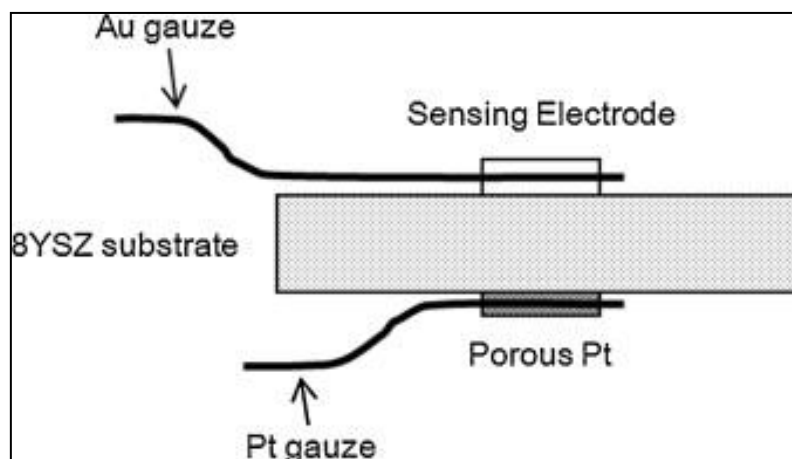
Figure 2-4: Schematic illustration of Potentiometric NOx sensors [12].

2.5   Impedancemetric Sensors

In comparison to the above mentioned potentiometric and amperometric NO_x sensors, the impedancemetric NO_x sensors are a relatively new and more promising approach towards achieving high NO_x sensitivity at low NO_x concentrations along with high selectivity and accuracy. This type of sensor is used in this thesis. In such sensors, the sensing response can be exhibited by impedance parameters such as the

modulus |Z| or phase component θ of the response of impedancemetric against an applied frequency. However, the angular phase component of the impedance, θ, is often more responsive to the changes in NO_x concentration [8, 13]. For this reason, it is frequently used to evaluate NO_x sensor sensitivity according to the mathematical expression **Eq. 2-2**:

$$\theta = arctan\frac{Z_R}{Z_I} \qquad \textbf{Eq. 2-2}$$

where Z_R and Z_I represent the real and imaginary components of the impedance, respectively. The impedance Z is defined accordingly:

$$Z(\omega) = Z_R + Z_I \qquad \textbf{Eq. 2-3}$$

The angular frequency $\omega = 2\pi f$ depends upon the applied sensor operating frequency, f. Advantages of the impedancemetric methods are total NO_x sensing is more readily achieved and the sensing response is highly reproducible in comparison to the potentiometric method. This approach is also a low-cost alternative to the amperometric method. In addition, NO_x sensing in the single digit ppm range is possible which exceeds the current amperometric NO_x sensing capability. A schematic diagram of an impedancemetric sensor is shown below.
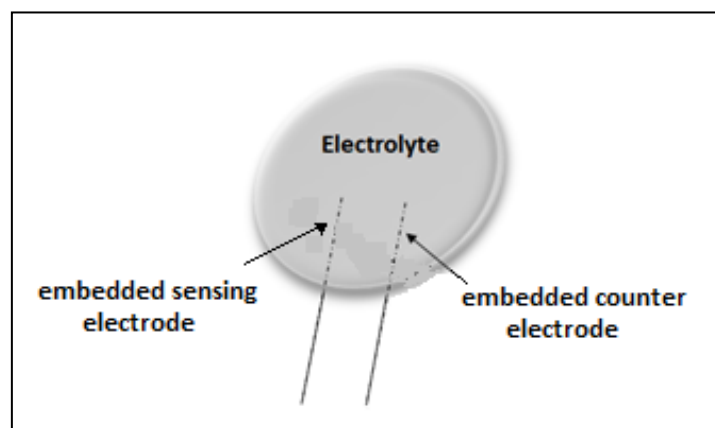
Figure 2-5: Schematic diagram of an impedancemetric sensor.

2.6   NOₓ Sensor Electrolyte

This thesis concentrates on electrochemical NO_x sensors supported by a zirconia (ZrO_2) based electrolyte. Zirconia has been used in NO_x sensors for decades because it tolerates the high temperature and stringent conditions of the exhaust environment. Zirconia is also chemically stable under lean (oxidizing) and rich (reducing) fuel conditions. Studies have found that the ionic conductivity of yttria - stabilized zirconia (YSZ) plays a role in electrochemical reactions that promote the sensitivity of the sensor to NO_x gases. The following paragraphs will discuss the chemical and microstructural properties of YSZ, and sensor reactions at the YSZ electrolyte and sensing electrode.

2.6.1   Chemical Structure of Zirconia

YSZ was first used by Nernst in 1899, when zirconia (ZrO_2) stabilized by yttria (Y_2O_3), illustrated the presence of ionic conductivity in solid state via oxide ionic vacancy (Vo) [14]. YSZ is a high temperature ceramic material commonly composed of the oxides of zirconium, yttrium, and in some cases silicon. Minor quantities of SiO_2 (~1%) are also added for suppressing the formation of grain boundaries. The valences of zirconium and yttrium differ by unity and they are found in the neighboring columns of the periodic table. The addition of yttrium (Y^{3+}) leads to the substitution of zirconium (Zr^{4+}) in the crystal lattice and, because of the valency difference, lattice defects (commonly known as vacancies) are developed for maintaining the electroneutrality. These lattice defects enable the YSZ electrolyte to transport oxygen ions from one vacancy to another and hence the electrolytic ionic conductivity is introduced [15].

In applications, such as NO_x sensors, the electrolyte may be in the form of a thick/thin film or pellet. In this case, the electrolytic ionic conductivity depends on the

electrolyte microstructure (i.e., porosity, particle size, and composition) as well as the sensor operating temperature [13, 16]. NO_x sensors have traditionally used NO_x sensitivity. In the case of porous electrolytes, the ionic conductivity is greater when the electrolyte porosity is low and the particles composing the electrolyte are uniform. This is because there are sufficient pathways for the oxygen ions to travel. However, it is important to note that low electrolyte porosity also limits the pathways for diffusion of exhaust gases, which can limit NO_x sensing reactions. Thus, it is necessary to establish a microstructure that balances ionic conductivity with other properties of the electrolyte.

The composition of the YSZ electrolyte depends upon the dopant concentration of yttria; also, adding another material to the electrolyte to form a composite can also modify the composition. Such changes to the electrolyte composition directly impact the electrolyte's conductivity. Modifying or tailoring the electrolyte's microstructure can be beneficial for enhancing the sensitivity and controlling the selectivity of the NO_x sensor.

The electrolyte's conductivity is temperature dependent. As the sensor's operating temperature increases, oxygen ions are able to travel more rapidly and reactions involving oxygen proceed more readily. It is important to note that there are multiple reactions occurring within the NO_x sensor that involve O_2, NO_x and other exhaust gases. Thus, selection of the preferred operating temperature for NO_x sensing must take into account not only the conductivity of the electrolyte, but also the temperature that promotes the desired NO_x reactions.

2.6.2   Electrochemical Electrolyte/electrode Interfacial Reaction

NO_x sensing reactions are understood to occur at the electrolyte/electrode interface. The porous electrolyte also allows for exhaust gases to participate at this

interface resulting in what is called a triple phase boundary (TPB). At the TPB, NO_x sensing reactions involving oxygen ions from the electrolyte, electrons from the electrode, and exhaust gases that diffused through the electrolyte pores to take place. As mentioned earlier, studies have found the porosity of the electrolyte affects gas transport to the (TPB) [2].

Sufficient porosity within the electrolyte allows gases to transport readily through the electrolyte. However, excess porosity can cause TPB reaction sites to become limited, which has the negative effect of decreasing NO_x sensitivity. Noble metals in the form of wires can be used as dense sensing electrodes. In this thesis, embedded Au wires were used as the sensing electrode. **Figure 2-6** illustrates the diffusion of gases through the grain boundary of the porous electrolyte along with the oxygen ions that travel through the bulk at the triple phase boundary reactions involving electrons from the Au wire electrode.
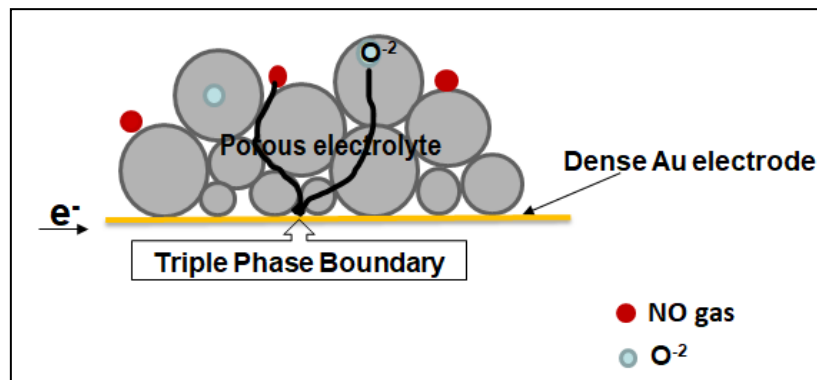
Figure 2-6: NO_x sensing reaction steps.

The primary equations describe TPB NO_x reactions as the following:

$$\tfrac{1}{2}\, O^{2-} + 2e^- \leftrightarrow O^{2-} \qquad \textbf{Eq. 2-4}$$

$$NO + O^{2-} \leftrightarrow NO_2 + 2e^- \qquad \textbf{Eq. 2-5}$$

$$NO_2 \leftrightarrow NO + \frac{1}{2} O^2 \qquad \textbf{Eq. 2-6}$$
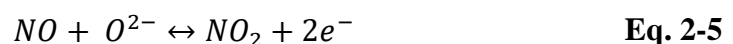
CHAPTER 3.

BASIC CONCEPTS OF ELECTROCHEMICAL IMPEDANCE SPECTROSCOPY

This chapter provides a discussion about the history and theory of electrochemical impedance spectroscopy (EIS), which is an important technique commonly used for analyzing the dynamics of charges (mobile and bound) within the bulk or at the interface of solid or liquid materials. The history of EIS can be traced back to 1880, when Oliver Heaviside introduced impedance spectroscopy to electrical engineering. Over the years, this technique was developed and improved by several scientists and three-dimensional analysis became possible in 1981. This technique is also useful for investigating the electrochemical characteristics of gas sensors, batteries, fuel cells and other electrochemical devices.

Impedance spectroscopy can effectively provide an understanding about the interdependency of NO_x reactions on the microstructure, composition, and material configuration of the NO_x sensors. EIS has developed rapidly since the 1960s because of the availability of newer, faster and more accurate measuring equipment. Impedance based sensors are similar in design to the potentiometric sensors, but at the place of voltage measurement, application of sinusoidal voltage and then measurement of resultant current is carried out. The ratio of this voltage and current is calculated in the frequency domain to give us the impedance response. This response is then analyzed to extract information about grain boundary resistivity and rates of chemical reactions. This analysis can also be used for further refinement and

quantification of chemical species. The most well-known investigation strategy for fitting EIS data is the utilization of equivalent circuit models using numerical models based on complex nonlinear slightest squares fitting.

As with every analysis methods, there are shortcomings to be aware of such as accuracy, expensive, and complex data analysis for quantification. The key limitation of EIS is the data can be difficult to interpret accurately due to overlapping time constants for various reactions. This can make it challenging to distinguish specific reaction mechanisms. Nonetheless, EIS is widely used because of the following benefits it provides:

- Non-destructive

- High quality data

- Running EIS is easy.

- EIS modeling analysis is very powerful.

- High information content

- Responses can be measured over large time periods.

3.1 Impedance, Modulus, Phase Angle

A general AC circuit is shown in **Figure 3-1** as follows:
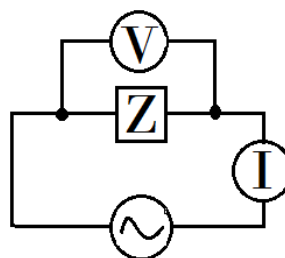
Figure 3-1: Illustration of a general AC circuit

Magnitude of impedance normally represented by symbol Z and is simply defined as the ratio of voltage to current. The data of impedance could be obtained in the following steps:

- In **Eq. 3-1**, E_t is the potential at time t, E_0 is the amplitude of the signal, and ω is the radial frequency. The relationship between radial frequency ω (expressed in radians/second) and frequency f (expressed in hertz) is $\boldsymbol{\omega = 2\pi f}$:

$$E_t = E_0 \, sin(\omega t) \hspace{3cm} \textbf{Eq. 3-1}$$

- The response signal, I_t, is shifted in phase (θ) and has a different amplitude than I_0 as the following equation, **Eq. 3-2**:

$$I_t = I_0 \sin(\omega t + \theta) \hspace{3cm} \textbf{Eq. 3-2}$$

- An expression analogous to Ohm's Law allows us to calculate the impedance of the system as **Eq. 3-3**:

$$\textbf{Eq. 3-3}$$
$$Z = \frac{E_t}{I_t}$$

The impedance is therefore expressed in terms of a magnitude, Z_o, and a phase shift, θ. **Figure 3-2** illustrates these crucial concepts.
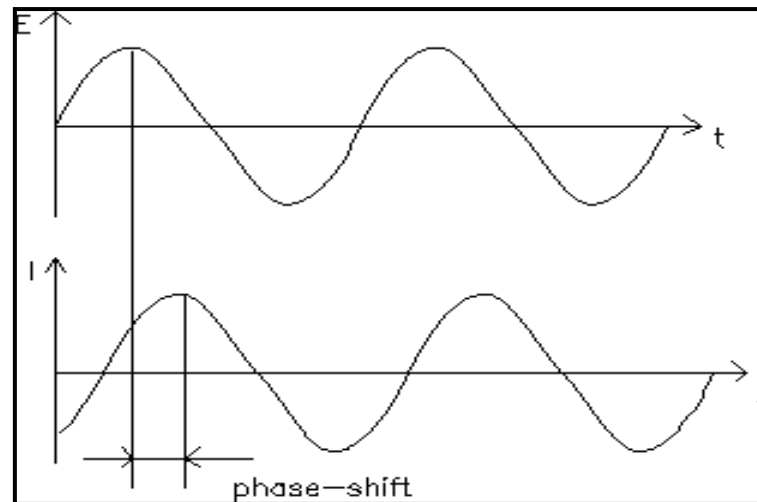
Figure 3-2: Illustration of fundamental concepts of EIS [17].

Impedance assumes an AC current of a specific frequency in Hertz. The impedance possesses components in both real and complex planes as given in **Eq. 2-3**.

The impedance data used to analyze the NO_x sensor response can be based on the following parameters (**Figure 3-3**):

- Frequency (Hz): the frequency of the applied sinewave.

- Time (s): the time coordinate corresponding to the measured data point in the spectrum.

- Z, modulus (Ohm): the modulus of the measured impedance as the following equation, **Eq. 3-4**:

$$|Z| = \sqrt{(Z')^2 + (Z'')^2}$$ **Eq. 3-4**

- Z', real part (Ohm): the real part of the measured impedance.

- -Z", imaginary part (Ohm): the imaginary part of the measurement impedance.

- -Phase (°): the phase shift.

The phase angle quantifies the lag or lead of applied voltage and output current at a specific frequency. It is commonly used as a sensing signal for NO_x sensors because of its better sensitivity and stability in comparison to the modulus. It is defined as the ratio of the impedance's real and imaginary parts as given in **Eq. 2-2**.
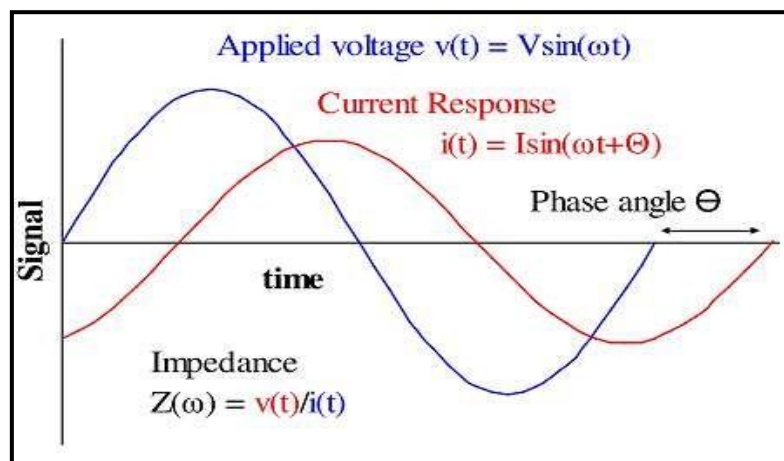
Figure 3-3: Fundamental concepts of Impedance Spectroscopy.

3.2   Representation of EIS Data

EIS data may be presented as a *Complex Plane (Nyquist) Plot* or a *Bode Plot*. A Nyquist plot is commonly used for representation of impedance data on a complex impedance plane. This plot provides a quick overview of the impedance data and qualitative interpretations could be made. The real as well as the imaginary axis are equal for avoiding distortion of the data curves. This plot is also called the Cole-Cole plot and its typical form is shown in **Figure 3-4**.
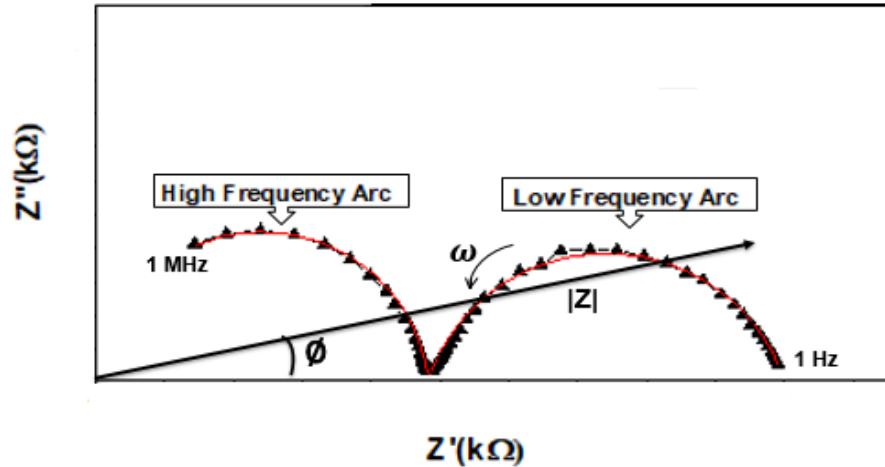
Figure 3-4: A typical Nyquist plot.
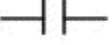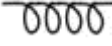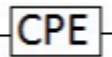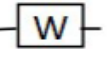
In practice, it is not uncommon for multiple and distorted arcs to be present in the impedance spectra. Each arc describes a relaxation process (frequency-dependent) in response to an input voltage signal. Furthermore, each arc in the spectra relates to at least one rate limiting reaction step. Impedance arcs occurring over the high frequency domain generally indicate that electrochemical reactions (e.g., charge transfer) are rate limiting. Arcs displayed in the low frequency regime suggest surface related processes are limiting. Analysis of the activation energy and oxygen partial pressure dependence can help to interpret rate-limiting processes. Correlating the rate limiting process with the microstructure of the sensor is expected to enable optimization of the fabrication process to reduce or eliminate rate-limiting mechanisms and promote NO_x sensor performance.

3.3 Equivalent Circuit Analysis

The basic purpose of an equivalent circuit is to model the impedance response generated by an electrochemical system. Equivalent circuit analysist can be used to interpret the underlying physical processes taking place at the electrode-electrolyte interface of a sensor. In normal practice, two or more parallel circuits are used for

properly explaining the output response of a sensor. Commonly used circuit elements include resistors, capacitors, and inductors, which are the ideal circuit elements. Some other elements such as Warburg diffusion and constant phase elements are also used, but they are non-ideal elements that compensate for deviations from ideal resistance and capacitance behavior. The details of the circuit elements are given in the following table.

Table 3-1: Elaboration of circuit elements [18].

Element	Circuit Symbol	Symbol	Significance
Resistor		R	Resistance to charge transfer
Capacitor		C	Capacitance arising from double layer charge
Inductor		I	Stray inductance
Constant Phase Element		Q	Non-ideal capacitor
Cole		RQ	Charge transfer through the double layer of the electrode / electrolyte.
Warburg		W	Infinite or semi-infinite electrode diffusion
Voigt		RC	Interfacial charge exchange

As shown in the above table, the Cole and Voigt are compound elements made by the combination of two single elements, RQ and RC, respectively. Normally, a modified form of Voigt element is used, which is also referred to as the Cole circuit in the series [18], as shown in the following figure:
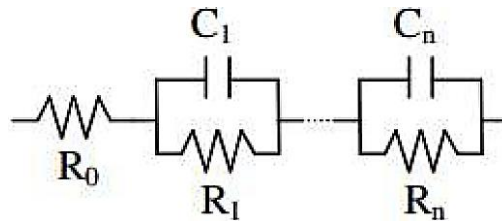
Figure 3-5: Voigt elements the in series.

The following chapters discuss impedancemetric NO_x sensor studies that were carried out using porous zirconia based electrolytes. The objective was to acquire a fundamental understanding of the role of microstructure and ionic conductivity on the NO_x sensing response. Towards this aim, NO_x sensors composed of various composite electrolytes were operated under different conditions to evaluate the relationship between electrolyte properties and NO_x sensor behavior.

CHAPTER 4.

EFFECT OF AL₂O₃ IN POROUS ZIRCONIA ELECTROLYTES FOR NO SENSING [1]

4.1   Overview

Porous electrolyte based NO_x sensors are under consideration for impedancemetric [19-23] and potentiometric [12, 24, 25] exhaust gas sensing applications. Enhanced NO_x sensitivity has been observed at such sensors, which typically incorporate electrodes with a dense microstructure. The porous electrolyte supports gas diffusion, while the dense electrodes limit heterogeneous catalysis reactions that interfere with accurately sensing NO and NO_2. These studies have largely concentrated on porous electrolytes composed of fully-stabilized yttria-doped zirconia (YSZ) due to the high ionic conductivity of the material that is known to promote NO_x sensitivity.

However, the porous YSZ microstructure and brittle nature of the ceramic limits sensor durability. Partially-stabilized yttria-doped zirconia (PSZ) has superior mechanical properties, in comparison to YSZ as the fracture toughness and impact resistance is greater [26]. PSZ has been considered as an alternative electrolyte in thin-film solid oxide fuel cells, as well as a composite anode component [27, 28].

---

[1] This material has been published as Kharashi, K. and Murray, E.P., 2016. "Effect of Al_2O_3 in Porous Zirconia Electrolytes for NO sensing". Journal of The Electrochemical Society, 163(13), pp. B633-B637 and is being reproduced with the kind permission of the publisher (The Electrochemical Society) and co-author.

Although the mechanical properties of PSZ are beneficial, they are also accompanied by reduced ionic conductivity, with respect to YSZ [29].

Adding small amounts of Al_2O_3 to yttria-stabilized zirconia can enhance ionic conductivity along the grain boundaries [30]. The reason is because Al_2O_3 is able to prevent impurities such as SiO_2 from blocking grain boundary transport pathways. Al_2O_3 additions can also contribute to the mechanical strength of the electrolyte [31], increase crystallographic phase stability [32], and limit hydrothermal aging [30]. Numerous studies reported a decrease in ionic conductivity when the Al_2O_3 addition to the electrolyte was greater than 2 wt%, since Al_2O_3 is an electrical insulator [30, 31, 33].

The mechanical and electrical properties of PSZ-Al_2O_3 composites are attractive for porous electrolyte based NO_x sensors, yet little is known about the role of Al_2O_3 for such applications. Impedancemetric NO_x sensing is a promising technique for achieving high accuracy NO_x detection at lower manufacturing costs, in comparison to the current commercial methods. Impedancemetric NO_x studies have reported similar gas sensing responses for NO and NO_2 as thermodynamic conversion causes NO_2 to convert to NO at elevated temperatures [34].

Thus, in the present study, the impedancemetric NO sensing response of porous PSZ based sensors with Al_2O_3 additions of 2, 3.8, 5, and 10 wt.% was analyzed for various operating conditions. The goal of the study was to gain greater understanding of the impact of Al_2O_3 on the porous electrolyte structural characteristics, electrical behavior of the sensors, and NO sensitivity.

4.2   Experimental

In this study, NO_x sensors were fabricated with PSZ electrolytes containing various amounts of alumina, along with embedded electrodes. Standard ceramic

processing methods were used to combine the PSZ electrolyte powder that was 8

wt.% (~4.7 mol.%) $Y_2O_3 - ZrO_2$ manufactured by UCM Advanced Ceramics with

high purity aluminum oxide (Al_2O_3) purchased from Sigma Aldrich. The 4 types of

PSZ-Al_2O_3 electrolytes fabricated contained 2, 3.8, 5, and 10 wt.% Al_2O_3.

The PSZ-Al_2O_3 powders were ball milled with 3 wt.% of polyvinyl butyral B-

76 binder and ethanol for 16 hours. A portion of the resulting PSZ- Al_2O_3 slurry was

dried and uniaxially pressed at 200 MPa into pellets with a diameter of 13 mm and

thickness of 3 mm. Au wire electrodes (0.25 mm diameter) covered with Au mesh to

enhance the current collection were coated with the remaining PSZ-Al_2O_3 slurry. The

Au mesh dimensions were 3 mm × 3 mm with an open area of 56.3%. PSZ

electrolytes without Al_2O_3 were fabricated by the same methods.

The sensor diagram given in **Figure 4-1** illustrates the placement of the

embedded electrodes. The diagram shows an uncoated view of the Au wires that were

6 mm apart with a 3 mm space between the Au mesh. The uncoated view is only for

illustration purposes as the Au mesh and Au electrodes were coated with a PSZ-Al_2O_3

slurry. The sensors were fired in air at 1050°C for 1 hr. Some PSZ and PSZ-Al_2O_3

electrolyte pellets without the Au wire electrodes were fired under the same

conditions and reserved for microstructural analysis in order to evaluate the impact of

Al_2O_3 addition within the sensor electrolyte. The porosity, morphology, and structural

characteristics of the PSZ and various PSZ-Al_2O_3 electrolyte pellets were analyzed

using Archimedes method, Scanning Electron Microscopy (SEM) and X-ray

Diffraction (XRD).

The impedancemetric response of the sensors was studied using a Gamry

Reference 600. Measurements for each sensor were conducted within a quartz tube

that was placed in a furnace where the operating temperature ranged between 550–

700°C. Mass flow controllers were used to manage the testing gas concentrations where NO ranged from 0-100 ppm with 1–18% O_2 present and N_2 as the balance gas. The total gas flow rate was 100 standard cubic centimeters per minute (sccm).

Data were collected for dry gas measurements, as well as humidified gas conditions where a water bubbler was used to establish a humidity of approximately 3%. The impedance measurements were collected at an applied signal amplitude of 50 mV over a frequency range of 1 Hz–1 M Hz. Measurements were repeated at least three times to ensure stable, reproducible results were achieved. Equivalent circuit analysis was used to aid interpretation of the electrochemical behavior of the NO sensors with respect to the Al_2O_3 concentration within the electrolyte.
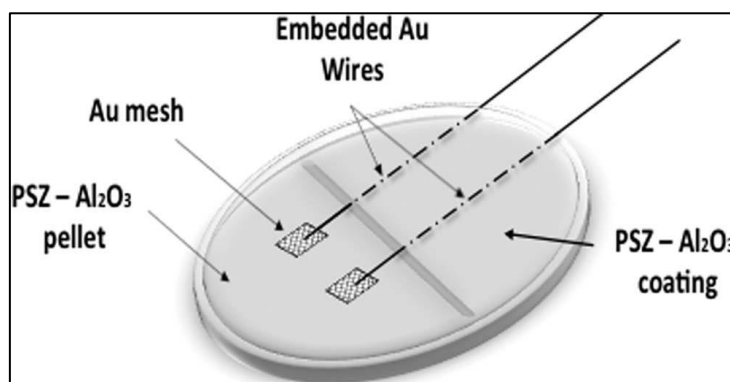
Figure 4-1: Schematic of NO sensor.

4.3   Results and Discussion

4.3.1   Microstructure and Morphology

Typical SEM cross-sectional images of fractured porous electrolyte pellets composed of PSZ and PSZ-2% Al_2O_3 are shown in **Figure 4-2**. These images were collected at an accelerating voltage of 1.0 kV using secondary electrons. Significant particle-to-particle contact was observed between PSZ particles that had necked together (Figures 4-2a–4-2b). Also, there were numerous pores well distributed throughout the PSZ electrolyte that tended to be 50–200 nm in size. The PSZ-2%

Al_2O_3 electrolyte image was typical of pellets with Al_2O_3 addition (Figures 4-2c–4-2d). The PSZ-Al_2O_3 composite pellets contained irregular shaped Al_2O_3 particles that were approximately 0.4–0.6 μm large. Given the low firing temperature (i.e. 1050°C), the Al_2O_3 particles did not coalesce with each other. Rather PSZ particles formed a network of contacts between Al_2O_3 and other PSZ particles. The pores within the PSZ-Al_2O_3 electrolytes appeared to be similar to those within the PSZ electrolytes.

The porosities of the electrolyte pellets were determined by using the Archimedes measurements. According to the Archimedes principle, a body submerged in a liquid will experience an upward force equal in magnitude to the weight of the liquid displaced by that body. This force is opposite to the direction of the gravitational force and could be given by the relation as follows:

$$F_B = m_f g \qquad \textbf{Eq. 4-1}$$

In the above equation, F_B is the upward or buoyant force and m_f is the weight of the liquid space by the body. A body floats in a fluid if the magnitudes of buoyant and gravitational forces become equal to each other. In this study, the determination of porosity was based on Archimedes' principle. This method involved the weighing of dry electrolyte pellets (W_{dry}) and then saturation of electrolytic pores by immersing it in a liquid. The weight of the submerged pellet (W_{sub}) was also noted, and then its saturated weight (W_{sat}) was determined after taking it out of the liquid. The porosity (φ) was then calculated by using the following relation:

$$\varphi = \frac{W_{sat} - W_{dry}}{W_{sat} - W_{sub}} \qquad \textbf{Eq. 4-2}$$

This liquid saturation method offers a simple way of calculating the porosity of electrolyte pellets. However, its major drawback is its low accuracy due to the incomplete saturation of the pore network. The porosity is generally defined as the volume of small spaces or voids that a porous material contains as compared to the

total amount of that material [35]. It is usually expressed in parentages and its relation

is given as follows:

$$Porosity = \frac{Volume\ of\ spaces\ or\ voids}{Total\ volume\ of\ the\ material}$$

Eq. 4-3

Archimedes measurements of the electrolyte pellets indicated the porosity was

about 44% for the PSZ pellets, and the porosity decreased with increasing Al_2O_3

addition. Porosity values for the PSZ- Al_2O_3 pellets are given in **Table 4-1**. The

decrease in porosity indicated Al_2O_3 particles blocked existing gas transport pathways

within the PSZ electrolyte. Other studies have found that the NO_x sensor electrolyte

porosity has a strong influence on the electrical response of the sensor [34]. Thus, the

Al_2O_3 electrically insulating particles also modified the ionic transport path- ways

within the sensor electrolyte.

Table 4-1: PSZ electrolyte porosity with respect to Al_2O_3 addition.

Electrolyte pellet	Porosity [%]
PSZ	44 ± 0.5
PSZ - 2% Al_2O_3	43 ± 0.5
PSZ - 3.8% Al_2O_3	42 ± 1.0
PSZ - 5%A Al_2O_3	41 ± 0.35
PSZ - 10% Al_2O_3	40 ± 0.10

Figure 4-2 shows XRD results for the PSZ and PSZ-Al_2O_3 composite pellets,

as well as the as-received Al_2O_3 powder. The primary phases observed in the PSZ-

Al_2O_3 composites were α-Al_2O_3 and tetragonal ZrO_2. A small peak belonging to cubic

ZrO_2 was observed near $2\theta = 74.5°$. The diffraction patterns showed an increase in the

α-Al$_2$O$_3$ peak intensity with increasing alumina addition in the PSZ-Al$_2$O$_3$ composite electrolytes.
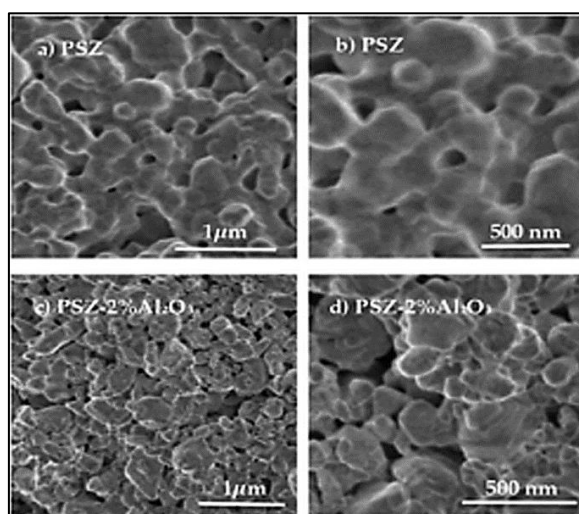
Figure 4-2:. SEM images of fractured cross-sections of electrolyte pellets illustrating typical: a) PSZ particle-to-particle contact b) PSZ microstructure at higher magnification, c) PSZ- Al$_2$O$_3$ composite with 2% Al$_2$O$_3$ addition, and d) PSZ-2% Al$_2$O$_3$ composite at higher magnification.
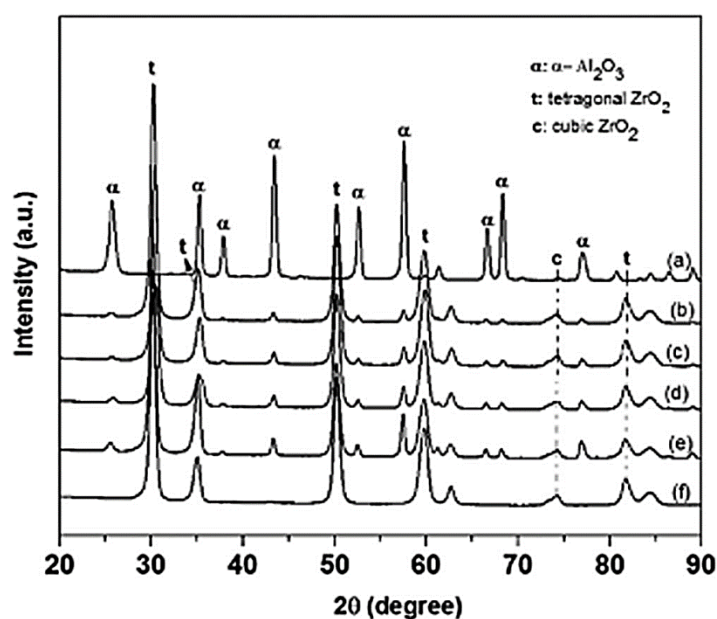
Figure 4-3: X-ray diffraction patterns for: a) Al$_2$O$_3$, b) PSZ-2% Al$_2$O$_3$, c) PSZ- 3.8% Al$_2$O$_3$, d) PSZ-5% Al$_2$O$_3$, e) PSZ-10% Al$_2$O$_3$, and f) PSZ.

4.3.2   Impedance response

Impedance spectroscopy measurements of the various sensors were collected to interpret the impact of Al_2O_3 as follows:

1) Electrical behavior of porous PSZ-Al_2O_3 electrolyte,

2) Interfacial NO reactions,

3) NO sensing response.

In **Figure 4-4**, the impedance data for sensors with a PSZ and PSZ-2% Al_2O_3 electrolyte illustrate the typical electrical response of sensors with and without Al_2O_3 addition. A partial high frequency arc and a distinct low frequency arc, respectively referred to as HFA and LFA, were present for both types of sensors. The partial arc described by HFA was due to electrolyte reactions, and electrode and interfacial reactions were described by the LFA. A comparison of the data indicated the total sensor impedance increased with the addition of Al_2O_3. In studies on the electrical behavior of Al_2O_3 added to yttria-stabilized zirconia, the bulk electrolyte ionic conductivity was found to decrease for additions of Al_2O_3 greater than 1 wt.% [30]. This decrease in ionic conductivity was correlated with a decrease in bulk electrolyte capacitance.

Thus, the increase in the HFA impedance that occurred when Al_2O_3 was added to PSZ likely resulted from a decrease in bulk electrolyte conductivity. The larger impedance of the LFA for the PSZ-2% Al_2O_3 based sensors can be attributed to insulating Al_2O_3 particles blocking electrochemical reaction sites along the triple-phase-boundary (TPB). The TPB is the location where the PSZ electrolyte, Au electrode, and gas phases were in contact. Al_2O_3 particles taking the place of PSZ particles along the TPB reduced the density of TPB reaction sites thereby, impeding interfacial reactions. Further analysis of the impedance response was carried out using

the equivalent circuit shown in **Figure 4-4**. It was used to model sensor impedance data. The circuit elements R_{HFA} and R_{LFA} represented the resistance of the HFA and LFA, respectively. The constant phase elements, CPE_1 and CPE_2, accounted for the non-ideal capacitance behavior of the respective HFA and LFA.
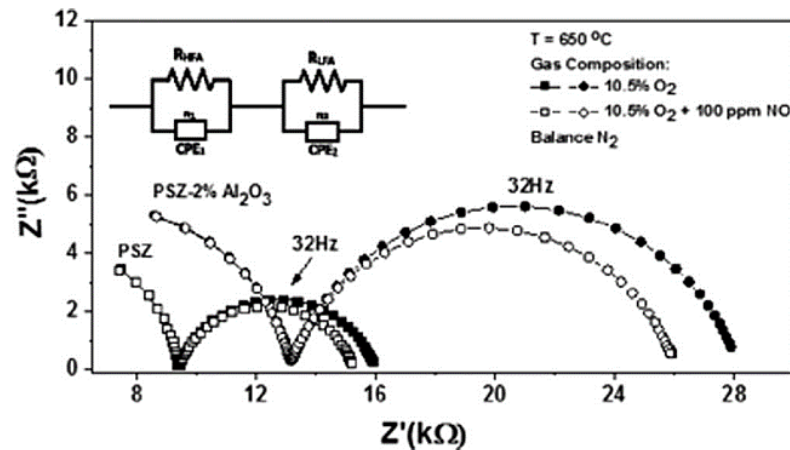
Figure 4-4: Impedance results of PSZ and PSZ-2%Al_2O_3 based NO sensors, and the equivalent circuit used for modeling.

The fitted values determined by equivalent circuit analysis for R_{HFA} and R_{LFA}, along with the magnitude of the impedance, |Z|, were used to generate the bar graph shown in **Figure 4-5** for sensors operating at 650°C.
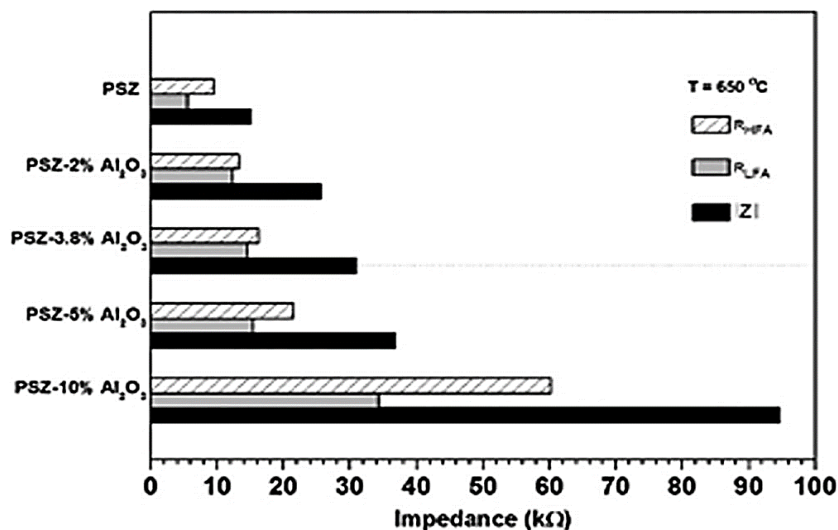
Figure 4-5: The fitted values from equivalent circuit modeling for R_{HFA}, R_{LFA}, and |Z| for impedance data collected at 650°C for PSZ and PSZ-Al_2O_3 based sensors.

The term $|Z|$ is defined by the real, Z_R, and imaginary, Z_I, impedance components as shown in **Eq. 3-4**. Here, the maximum value for $|Z|$ was the overall magnitude of the impedance, which corresponded to the sum of R_{HFA} and R_{LFA}. Details concerning the theory of $|Z|$ behavior are described elsewhere [36]. The R_{HFA} component was significantly larger than R_{LFA} for the PSZ based sensors. Reactions governed by the porous microstructure of the electrolyte as well as the bulk and grain boundary conductivity of PSZ contributed to the resistance modeled by R_{HFA} [37, 38].

For sensors containing 2 wt.% Al_2O_3, the corresponding values for R_{HFA} and R_{LFA} did not differ greatly. This result was possibly related to an enhancement in the electrolyte grain boundary conductivity that could have limited the resistance of R_{HFA}. Although Al_2O_3 additions can impede electrolyte bulk conductivity, it can have the opposite effect on the electrolyte grain boundary conductivity for Al_2O_3 additions ≤ 2 wt.% [30]. As the Al_2O_3 addition increased to 5 wt% in the PSZ-Al_2O_3 composite electrolyte, the $|Z|$ of the sensors gradually increased. This was likely related to an increase in electrolyte bulk and grain boundary resistivity resulting from greater Al_2O_3 additions, which in turn contributed to R_{HFA}. As for R_{LFA}, the modeled data indicated a subtle increase in value for Al_2O_3 additions of 2–5 wt.%, which suggested electrode and interfacial reactions were not significantly impeded.

When the amount of Al_2O_3 increased to 10 wt.%, a substantial increase in both R_{HFA} and R_{LFA} was observed for the corresponding sensors. Adding 10 wt.% Al_2O_3 to the electrolyte most likely hindered electrolyte reactions and interrupted PSZ contact along the TPB such that interfacial reactions were limited. The slight distortion of the impedance arcs from ideal semi-circles was accommodated by CPE_1 and CPE_2 fitting elements. Since the partial HFA described contributions from multiple electrolyte reactions, it was difficult to decipher specific phenomena associated with CPE_1 with

respect to Al_2O_3 addition. On the other hand, fitted valued associated with CPE_2 were found to decrease with Al_2O_3 addition. The capacitance associated with CPE_2 decreased from approximately 6.25×10^{-7} F for PSZ electrolyte based sensors down to about 1×10^{-7} F for sensors with 10 wt.% Al_2O_3. The following equation **Eq. 4-4** was used to determine the capacitance (C):

$$C = \frac{[(R_{LFA})(CPE_2)]^{1/n}}{R_{LFA}} \qquad \text{Eq. 4-4}$$

The constant n describes the deviation from pure capacitance behavior. For an ideal capacitor n = 1. Here, equivalent circuit modeling results indicated n $\sim$ 0.8 for the PSZ and PSZ- Al_2O_3 sensors. Operating the sensors under humidified gas conditions resulted in an increase in the impedance, specifically for the LFA, as shown in **Figure 4-6**.
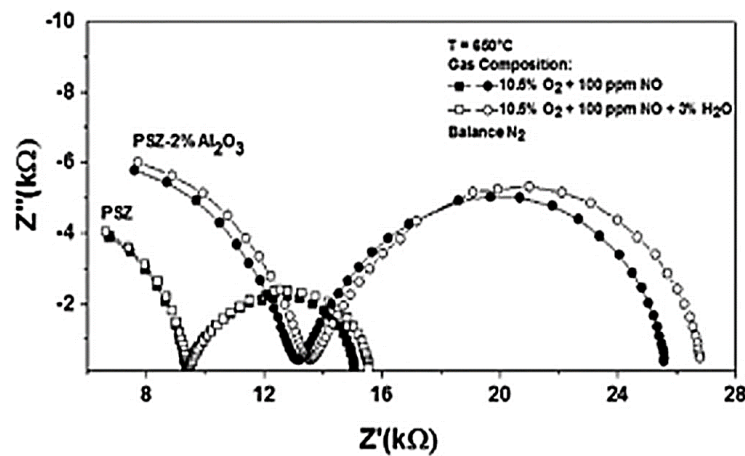
Figure 4-6: Impedance response of sensors under dry and humidified gas conditions.

The HFA behaved independent of gas concentration as it is controlled by temperature dependent reactions [36]. The behavior of NO_x sensors in the presence of water vapor can differ due to variations in material processing and operating conditions. Here, it is possible that gas species resulting from molecular water reactions occupied sites along the TPB, thereby reducing the availability of sites for oxygen and NO. Thus, limited TPB reactions may have contributed to a larger

interfacial resistance. Similar observations were observed for the various PSZ-Al_2O_3 sensors.

4.3.3   NO sensing

The impact of Al_2O_3 addition within the sensor electrolyte on impedancemetric NO sensing was evaluated based on the change in the angular phase response, $\Delta\theta$, according to **Eq. 4-5**:

$$\Delta\theta = \theta_{o2} - \theta_{NO} \qquad\qquad \textbf{Eq. 4-5}$$

where θ_{o2} was the sensor baseline angular phase response during operation with 10.5% O_2, and θ_{NO} was the response with added NO. The phase angle is useful for sensing NO [19] and is defined as the ratio of the real Z_R, and imaginary Z_I parts of the impedance at a specific frequency, $f = 2\pi\omega$, as given in **Eq. 2-2**.

Sensitivity to 100 ppm NO for the PSZ-Al_2O_3 based sensors with respect to operating temperature is shown in **Figure 4-7**. Automotive exhaust generally contains some amount of water, thereby creating humidified gas conditions that can impact NO sensitivity. Here, the sensitivity measurements with humidified gases were about 2% lower than dry sensitivity measurements. Data for the sensors with 10 wt.% Al_2O_3 addition were excluded for temperatures $\leq 600°C$ as the data was unreliable due to significant noise in the impedance response, particularly for lower frequencies. The poor data likely resulted from insufficient contact of PSZ at the TPB due to interference from Al_2O_3 particles.
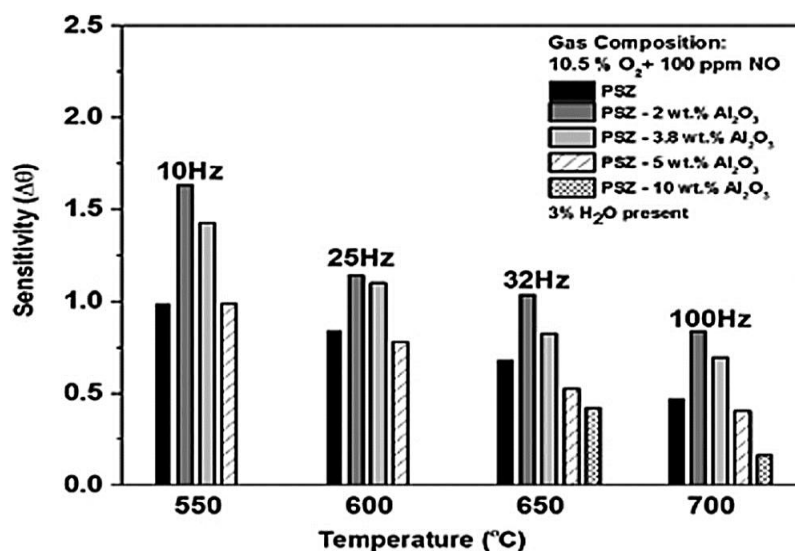
Figure 4-7: Sensitivity to 100 ppm NO for the PSZ and PSZ-Al_2O_3 based sensors.

Sensitivity data for each type of sensor were collected during operation at the peak frequency where the maximum phase angle response was achieved. The highest NO sensitivity was observed for the sensors composed of PSZ-2% Al_2O_3. The 2 wt.% Al_2O_3 addition to the PSZ electrolyte most likely contributed to enhanced conductivity along the PSZ grain boundaries that enabled electrochemical reactions involving oxygen ions and NO to proceed more readily. Sensitivity to NO decreased with increasing Al_2O_3 addition and operating temperature. Increasing the Al_2O_3 addition hindered the ionic conductivity, as well as the gas transport pathways within the sensor electrolyte, and subsequently reduced NO sensitivity. The increase in temperature may have enabled oxygen reactions to proceed more readily in comparison to NO reactions. The data presented in **Figure 4-7** also indicates the peak frequency increased with the sensor operating temperature.

Although sensor operation at 10 Hz and 550°C yielded the greater NO response, higher frequency operation would enable the sensors to operate more rapidly as the gas sampling time would be reduced [21]. A key aspect of sensor feasibility involves balancing the trade-off between the magnitude of the sensing signal and sensor

response time. The sensing behavior of PSZ-2% Al_2O_3 based sensors for various NO

concentrations under humidified conditions is shown in **Figure 4-8**.
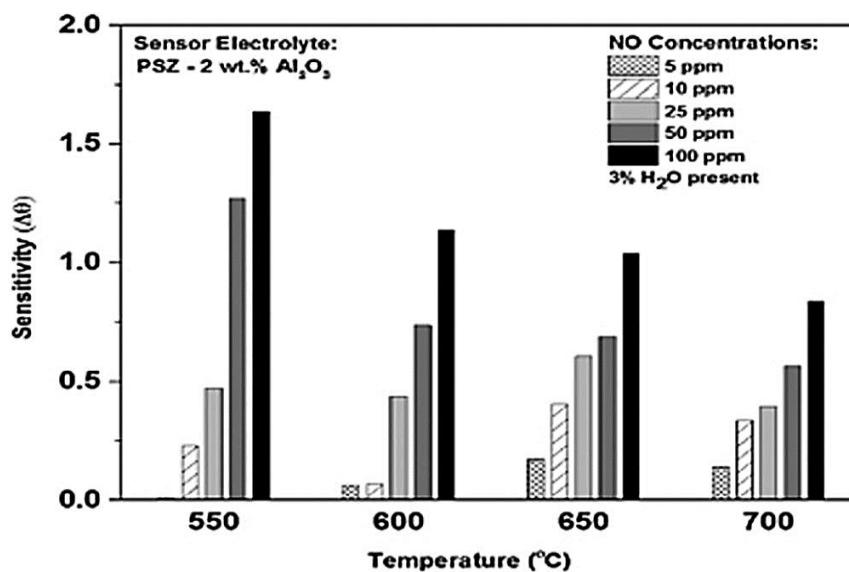
Figure 4-8: The sensing behavior of PSZ-2% Al_2O_3 based sensors for various NO concentrations under humidified conditions.

The peak frequency and corresponding operating temperatures were the same

as those given in **Figure 4-7**. The sensing response for NO concentrations of 5 ppm

was negligible when the operating temperature was $550°C$. As the operating

temperature increased the PSZ-2% Al_2O_3 based sensors were more sensitive to NO

concentrations ≤ 10 ppm. However, a decrease in NO sensitivity for all gas

concentrations was observed at $700°C$.

The data presented in **Figure 4-8** can be compared to other impedancemetric

studies by considering $\Delta\theta/\Delta[NO]$, where $\Delta\theta$ is given by the values along the y-axis

and $\Delta[NO]$ is the difference between the concentration of NO at baseline gas

conditions and the concentration of NO present. (In this study, the NO concentration

was 0 ppm for baseline gas conditions such that $\Delta[NO]$ was the NO concentration

introduced to the sensor).

For data collected at T = 650°C for the PSZ-2% Al_2O_3 based sensors $\Delta\theta/\Delta[NO] \approx 0.03$ degrees/ppm NO at an operating frequency of 10 Hz. Impedancemetric NO_x sensor studies by Woo *et al.* reported $\Delta\theta/\Delta[NO] \approx 0.07$ degrees/ppm NO for porous fully-stabilized Y_2O_3-ZrO_2 based sensors with a Au wire sensing electrode operating at 650°C [21]. This comparison indicates the fully-stabilized Y_2O_3-ZrO_2 based NO_x sensors are more sensitive to NO than the PSZ-2% Al_2O_3 based sensors for similar operating conditions. This was expected as the higher ionic conductivity of fully-stabilized Y_2O_3-ZrO_2 electrolyte promotes NO sensitivity. Increasing the ionic conductivity of the PSZ-Al_2O_3 by optimizing the amount of Al_2O_3 within the composite electrolyte may be a means to achieve greater NO sensitivity and sensor feasibility. A comparison of $\Delta\theta/\Delta[NO]$ calculations for PSZ and PSZ-2% Al_2O_3 based sensors were determined to be approximately 0.010 and 0.016 degrees/ppm, respectively for an operating frequency of 32 Hz. This indicates the 2 wt.% Al_2O_3 addition enabled about a 38% increase in NO sensitivity. Thus, determining the optimal concentration for the Al_2O_3 addition could potentially further improve NO sensing for PSZ-Al_2O_3 sensors.

4.3.4 PO_2 and E_a dependence

The oxygen partial pressure, P_{O2}, and activation energy, E_a, were determined in order to provide an understanding of potential rate limiting mechanisms affecting sensor behavior and the temperature dependence. NO_x sensing studies show that NO sensitivity is related to the rate limiting mechanism for oxygen [20]. Identifying the rate determining step for the oxygen reaction is important for understanding NO sensing behavior. The oxygen partial pressure is given by the power law relationship as given in **Eq. 4-6**:

$$(P_{O2})^m \propto R_{LFA} \qquad\qquad \textbf{Eq. 4-6}$$

where m is the slope. As shown in **Figure 4-9**, the PSZ based sensors had a PO_2

dependence where m = −0.47, and the corresponding activation energy was $1.03 \pm$

0.01 eV. Adding Al_2O_3 to the PSZ electrolyte caused the slope associated with PO_2 to

become more negative. The activation energy remained close to 1eV, although a

slight decrease was observed with increasing Al_2O_3 addition. For example, Ea

decreased to 1.01 ± 0.02 eV for the PSZ-5% Al_2O_3 sensors. Data for the PSZ-10%

Al_2O_3 sensors was not reliable at lower oxygen concentrations due to significant noise

observed in the response for reasons previously discussed.
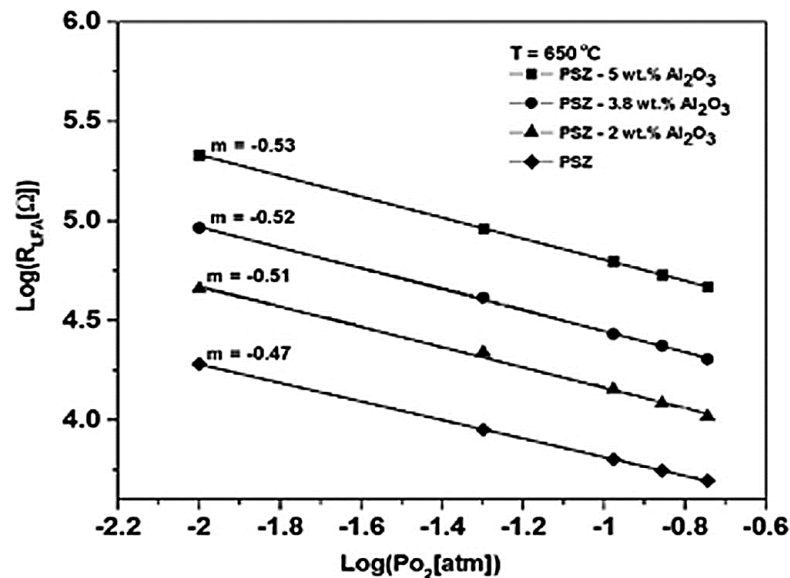
Figure 4-9: Effect of Al_2O_3 addition on the oxygen partial pressure dependence of the
various sensors.

Studies on Au/YSZ/Au NO_x sensors have calculated similar activation energy

values, and the PO_2 dependence followed a slope, $m \approx −0.5.\underline{18}$ A $PO_2^{-0.5}$ dependence

can be an indication that dissociative adsorption of oxygen is rate limiting [39, 40].

The slope value for the PSZ based sensors was slightly lower than m = −0.5, which

may indicate that an additional process was rate limiting. Since the charge transfer

step is associated with a $PO_2^{-0.25}$ dependence, it is possible that charge transfer at the

TPB was also a rate limiting process for the PSZ based sensors.

It has been shown in other studies that NO_x sensing was hindered significantly in sensors where charge transfer was the dominant limiting mechanism for the oxygen reaction, whereas NO_x sensing seemed to proceed more readily when dissociative adsorption was the rate determining step for oxygen [20, 23]. The Al_2O_3 addition to PSZ caused to oxygen partial pressure dependence to become more negative, which suggested gas phase diffusion began to have an impact. Other studies have found a $P_{O_2}^{-1}$ dependence is associated with gas diffusion [40]. The measured decrease in the electrolyte porosity of the sensors with addition of Al_2O_3 correlated with gas diffusion as an additional rate liming step due to Al_2O_3 addition.

4.3.5   Conclusions

The addition of Al_2O_3 to PSZ resulted in an increase in the NO sensor impedance. Adding 2 wt.% Al_2O_3 seemed to enhance the PSZ electrolyte grain boundary conductivity, which supported electrochemical NO reactions at the TPB. Increasing the Al_2O_3 addition above 2 wt.% in the PSZ electrolyte increased the resistance of the electrolyte bulk, grain boundaries and interfacial reactions. In addition, the decrease in porosity with Al_2O_3 addition restricted gas transport pathways within the porous electrolyte.

The dominant rate limiting mechanism for the PSZ-2% Al_2O_3 based sensors appeared to be oxygen dissociative adsorption, whereas oxygen dissociative adsorption combined with charge transfer or gas diffusion seemed to be rate limiting for PSZ and the other PSZ-Al_2O_3 composite based sensors. Overall, the addition of 2 wt.% Al_2O_3 to PSZ based sensors resulted in greater sensitivity to NO, and sensitivity was achieved at concentrations as low as 5 ppm NO.

CHAPTER 5.

MANAGING H₂O CROSS-SENSITIVITY USING COMPOSITE ELECTROLYTE NOX SENSORS [2]

5.1   Overview

Advancements in diesel engine technology and emissions regulations in various countries are driving the need for NO_x sensors capable of greater sensitivity, selectivity, and accuracy. Zirconia-based NO_x sensors are favored for their stability and electrochemical performance under stringent exhaust conditions. Various research studies have achieved substantial NO_x sensitivity at sensors utilizing novel porous electrolytes, as an alternative to the conventional dense electrolyte microstructure [19, 34, 41]. NO_x sensors based on the conventional architecture commonly have porous precious metal electrodes to support exhaust gas transport to the electrode/electrolyte interface where NO_x sensing reactions take place. Unfortunately, heterogeneous catalysis can occur within the porous electrodes, thereby reducing the amount of NO_x gas arriving at the interface. This becomes a significant problem when it is necessary to detect low concentrations (i.e., <10 ppm) of NO_x as sensor accuracy is compromised. Heterogeneous catalysis is negligible at NO_x sensors using a porous zirconia-based electrolyte with dense electrodes. The porous electrolyte does not appear to interfere with the exhaust gas during transport to the electrode/electrolyte interface. Thus, the

porous zirconia electrolyte enables greater NO_x sensor sensitivity and accuracy. However, cross-sensitivity to interfering exhaust gases, particularly water vapor, adversely affects the selectivity of the device. Sensor operation at specific frequencies appears to be an effective measure for addressing cross-sensitivity to oxygen [19]. Yet, this approach has not been effective for limiting cross-sensitivity to water. Greater understanding of the behavior of water during sensor operation is necessary for managing water cross-sensitivity and improving the feasibility of porous zirconia-based NO_x sensors.

Cross-sensitivity in NO_x sensors can result from electrochemical reactions with exhaust gas species that proceed more readily and/or more rapidly than NO_x reactions. Accumulation of various molecules at the electrode/electrolyte interface can also enable undesirable reactions to proceed leading to cross-sensitivity. The impact of water cross-sensitivity has been ambiguous as it can cause the NO_x sensing response to increase or decrease [42-44]. Some studies suggest that the different behavior observed is related to the sensor materials, fabrication methods, and operating conditions. Few studies have reported the NO_x sensing response for various water concentrations. Limited data with varying results has made it difficult to understand and control the impact of water on the sensing behavior of porous electrolyte NO_x sensors.

Recently, the authors found composite electrolyte NO_x sensors with a porous microstructure demonstrated reduced cross-sensitivity to water in comparison to sensors with a single-phase electrolyte. To further study the potential of composite electrolytes for NO_x sensing, various sensors based on electrolytes containing specific ratios of partially stabilized zirconia (PSZ) and fully stabilized zirconia (FSZ) were evaluated using the impedancemetric technique. The work presented in

this chapter describes the electrochemical response, gas sensitivity, rate limiting mechanisms, and sensing response rate due to operation in humidified gas environments for composite electrolyte NO_x sensors.

5.2   Experimental

Standard ceramic processing techniques were used to fabricate NO_x sensors containing partially-stabilized zirconia (PSZ, 4.7 mol.% $Y_2O_3–ZrO_2$) produced by advanced ceramics and fully stabilized zirconia (FSZ, 8 mol.% $Y_2O_3–ZrO_2$) manufactured by Tosoh as electrolyte materials. There were five electrolyte slurries prepared using different ratios of PSZ and FSZ along with polyvinyl butyral (Butvar B-76) binder and ethanol for the solvent. The slurries were ball milled for 16 hours to form a uniform mixture. A portion of each electrolyte slurry was dried and the powders were pressed uniaxially at 200 MPa into pellets. The three types of PSZ–FSZ composite electrolytes studied contained 25, 50, and 75 vol.% PSZ, and are identified as 25 PSZ–75 FSZ, 50 PSZ–50 FSZ, and 75 PSZ–25 FSZ, respectively.

Electrolytes composed of single-phase FSZ or single-phase PSZ particles were fabricated for performance comparison purposes. Single-phase PSZ electrolytes containing coarse particles were also fabricated in order to study the impact of particle size on water cross-sensitivity. Gold (Au) electrodes were placed over the electrolytes and coated using the corresponding electrolyte slurry to complete the sensor configuration. The sensors were air dried and then fired at 1050°C for a period of 1 hour.

A schematic of the top view and cross section of the sensors is shown in **Figure 5-1**. The top view shows the position of the sensor electrodes without the electrolyte coating. The cross-sectional view includes the electrolyte coating over the electrodes. There was no distinction observed between the electrolyte coating and

pellet as the materials were of the same composition. The microstructure and morphology of the electrolytes were analyzed using scanning electron microscopy (SEM) and Archimedes method.

The electrochemical behavior of the sensors was characterized using a Gamry Reference 600 to perform impedance spectroscopy. Impedance measurements were performed for sensors operating over a temperature range of 600–700°C where the concentration of NO and NO_2 was varied from 0 to 100 ppm in O_2 concentrations of 1–18% with N_2 as the balance. Data was collected for dry and humidified (3–10% H_2O) environments using a standard gas handling system with mass flow controllers that maintained a flow rate of 100 standard cubic centimeters per minute (sccm). The Gamry instrument was configured to apply a signal amplitude of 50 mV over an operating frequency range of 1 Hz^{-1} MHz. Measurements were collected in triplicate to ensure the data was consistent and stable. Equivalent circuit modeling using Gamry EIS300 software was used to acquire a detailed understanding of the electrochemical behavior of the sensors.
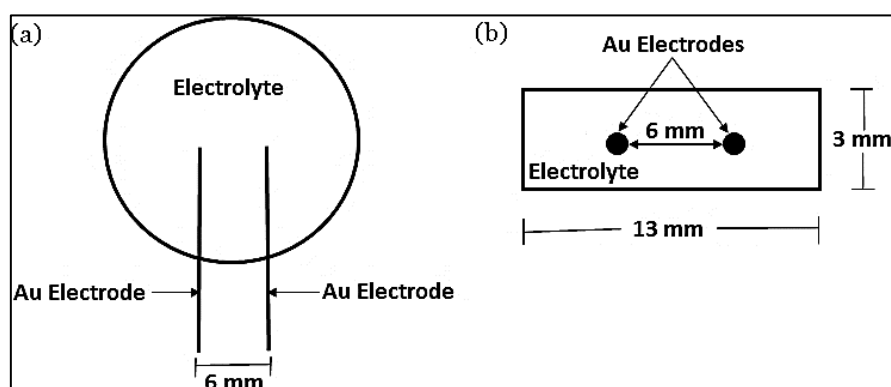
Figure 5-1: NOx sensor diagram: (a) top view, and (b) cross-sectional view with embedded Au wire electrodes.

5.3   Morphology and Microstructure

The microstructure of the porous electrolyte can impact gas sensor reactions. Studies have found the porosity of the electrolyte affects gas transport to the triple

phase boundary (TPB) [34, 37]. The TPB is the location where the electrolyte, electrode, and gas phase are in contact. The TPB is important as NO_x sensing reactions take place along this boundary. Insufficient porosity within the electrolyte restricts gas transport to the TPB and limits sensor reactions. This usually results in a slow sensor response rate that is not practical for automotive applications. On the other hand, excess porosity allows gases to transport readily through the electrolyte, but also causes TPB reaction sites to become limited, which has the negative effect of decreasing NO_x sensitivity.

Figure 5-2 shows typical SEM surface images for PSZ, FSZ, and PSZ–FSZ composite electrolytes. The particles composing the PSZ electrolytes in **Figure 5-2**a were irregular in shape and varied from 0.1 to 0.3 µm in size, whereas the FSZ electrolytes consisted of finer particles that seemed to be more uniform in size (largest diameter ∼0.04 µm) and shape. The FSZ particle-to-particle connectivity, shown in **Figure 5-2**b, appeared to be greater than the particle connectivity between PSZ particles. The PSZ–FSZ composite electrolytes contained a well-distributed mixture of PSZ and FSZ particles, as shown in **Figure 5-2**c. In addition, larger pores were observed throughout the composite microstructure in comparison to the single-phase electrolytes. **Figure 5-2**d shows an image of the microstructure of electrolytes containing PSZ coarse particles where the particle size ranged from about 0.4–1 μm. **Table 5-1** gives the porosity measurements for the various electrolytes that were determined via the Archimedes method. The irregular shaped PSZ particles allowed for closer packing of the particles, thereby lowering the porosity of PSZ-based electrolytes.
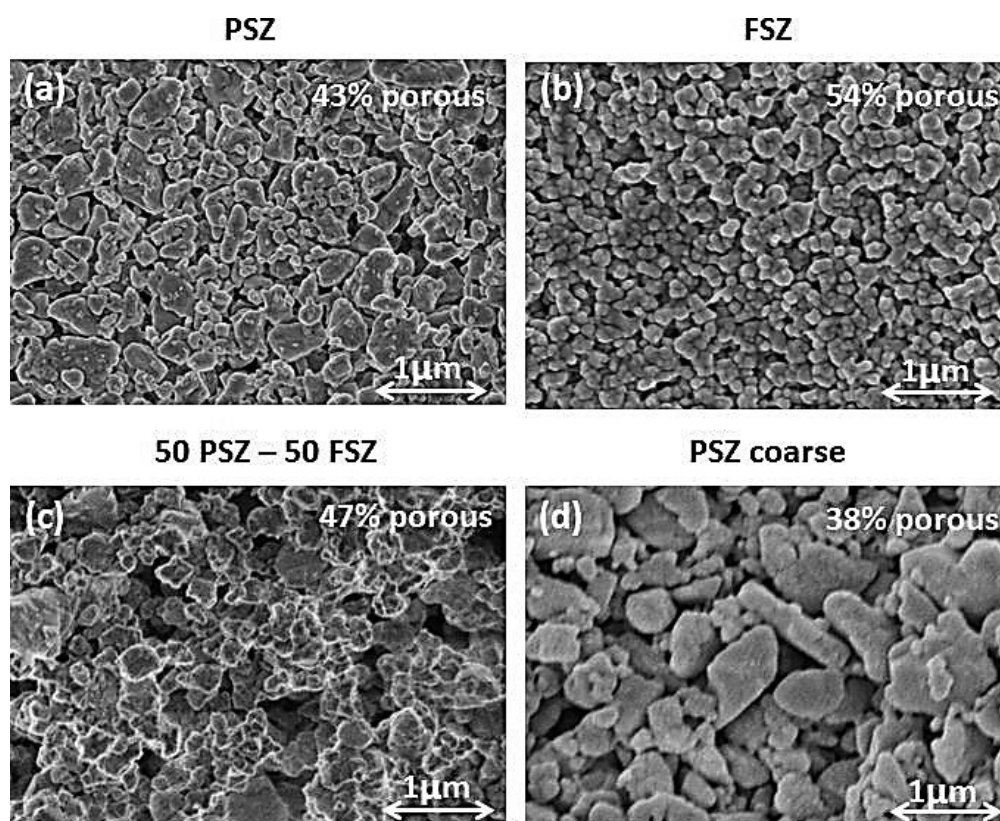
Figure 5-2: SEM images of electrolytes composed of: (a) PSZ, (b) FSZ, (c) 50 PSZ–50 FSZ, and (d) PSZ coarse particles.

Table 5-1: Electrolyte porosity based on the Archimedes Method.

Electrolyte Porosity					
PSZ	75 PSZ - 25 FSZ	50 PSZ - 50 FSZ	25 PSZ - 75 FSZ	FSZ	PSZ course
43 %	45 %	47 %	50 %	54 %	38%

5.4 Electrochemical Response

Impedance spectroscopy is a powerful and commonly used technique for interpreting the electrical response of electrochemical devices and systems [36]. The impedance is an AC measurement that describes the opposition to the current's flow due to resistance, inductance, and capacitance effects. The impedance, $Z(\omega)$, varies with frequency, f, and is generally represented by **Eq. 2-3**.

where the angular frequency $\omega = 2\pi f$. In addition, the real (Z_R) and imaginary (Z_I) impedance typically produce a semicircular shaped response or arc that is presented in the complex plane. In practice, more than one arc is common due to various reactions occurring at different rates. The impedance measurements for the NOx sensors in this work consisted of a high and low frequency arc. The high frequency arc (HFA) described electrochemical reactions occurring at the porous electrolyte, and the low frequency arc (LFA) reflected electrode and interfacial reactions.

Figure 5-3 shows typical impedance data describing the electrochemical response of PSZ, FSZ, and 50 PSZ–50 FSZ-based sensors operating at 600°C with and without 100 ppm NO present under dry and humidified conditions. Data for sensors composed of PSZ coarse particles is included. For each type of sensor, the high frequency arc was independent of the gas concentration. In addition, the magnitude of the high frequency arc differed on account of the difference in ionic conductivity for PSZ (~0.08 S/cm) versus FSZ (~0.14 S/cm) [29]. The higher conductivity of FSZ contributed to the lower high frequency arc impedance. Thus, the magnitude of the high frequency arc decreased as the FSZ composition within the sensor increased. These observations were expected as the high frequency arc is known to depend upon the ionic conductivity and operating temperature of the electrolyte material [36]. In all cases here, the high frequency arc was incomplete on account of the high frequency limitation of the Gamry Reference 600 instrument.

As the high frequency arc does not vary with gas concentration, it is generally not useful for interpreting the sensor response to NO_x gas reactions. Therefore, acquiring a complete high frequency arc was not necessary for this study. For the low frequency arc, there was a decrease in magnitude when 100 ppm NO was added to the gas stream as shown in **Figure 5-3** for each sensor type. This change indicated

electrode and interfacial reactions proceeded more readily when NO was present. The impedance data for sensors operating with 100 ppm NO_2 gas was very similar to that for NO. Thermodynamic conversion of NO_2 to NO takes place at elevated temperatures, such that at 600°C approximately 90% of NO_2 converts to NO.
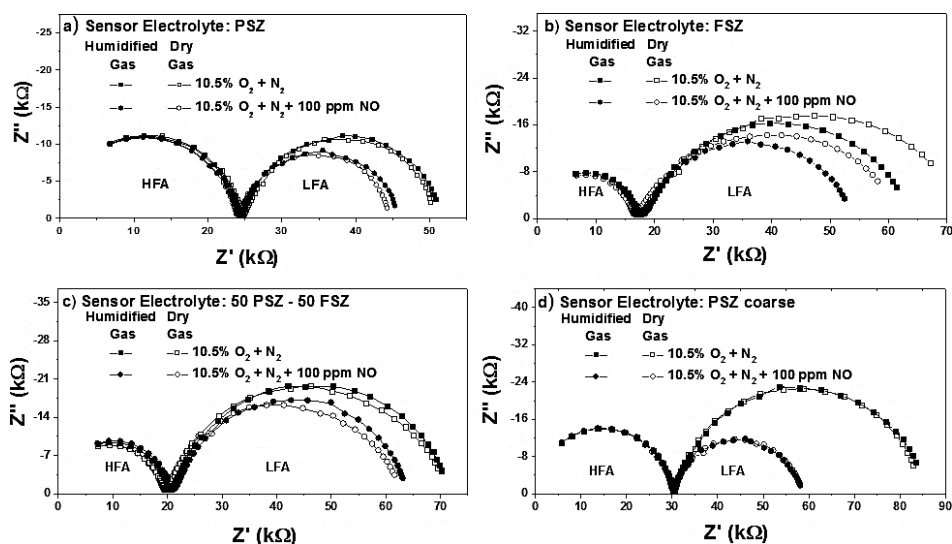
Figure 5-3: Impedance data collected at 600°C where the sensor electrolyte was: (a) PSZ, (b) 50 PSZ–50 FSZ, (c) FSZ, and (d) PSZ coarse under dry and humidified conditions.

For this reason, data using NO gas is presented in this work. The addition of water to the gas stream caused the low frequency impedance arc to decrease slightly for sensors with a PSZ, 75 PSZ–25 FSZ, and 50 PSZ–50 FSZ electrolyte. Quite the opposite behavior occurred for sensors containing a FSZ and 25 PSZ–75 FSZ electrolyte. The change in the impedance due to water cross-sensitivity is shown for sensors composed of PSZ, FSZ, and 50 PSZ–50 FSZ in **Figure 5-3**a–c. In other studies, analysis of water adsorption experiments at oxide surfaces have found that molecular water strongly adsorbs onto the surface of Y_2O_3 and surface reactions result in the formation of hydroxyl groups [40, 45].

Furthermore, computational studies indicate dissociation of water molecules is a mechanism for the formation of hydroxyl species at Y_2O_3–ZrO_2 surfaces, and

interfacial reactions between the oxide and hydroxyl groups can enhance oxygen ion conductivity [46]. However, it is also possible for adsorbed water molecules and hydroxyl species to block oxygen adsorption sites along the electrolyte/electrode interface and subsequently hinder interfacial reactions with oxygen [43].

In the present study, the Y_2O_3 content of the sensor electrolyte was approximately 4.7 and 8 mol.% for PSZ and FSZ supported sensors, respectively. It is possible that the higher Y_2O_3 content of FSZ allowed greater adsorption of molecular water and hydroxyl groups to take place at sensors containing an FSZ based electrolyte in comparison to sensors with ≥50 vol.% PSZ. This would decrease the available sites for NO and O_2 adsorption. For such a case, triple-phase-boundary reactions requiring NO and O_2 would be limited, thereby causing the sensor impedance to increase in the presence of water, as shown in **Figure 5-3**b. The slight decrease in impedance for PSZ sensors likely occurred due to enhanced oxygen ion conductivity. The lower Y_2O_3 content of PSZ possibly resulted in less molecular water coverage such that sufficient adsorption of oxygen was able to take place. The adsorbed oxygen along with resulting hydroxyl species participated in reactions that produced oxygen ions, which enabled triple-phase-boundary reactions to proceed more readily at PSZ-based sensors.

As mentioned previously, the microstructure of the sensor electrolyte affects the number of particles and reaction sites along the triple-phase-boundary where NO_x reactions take place. The SEM images in **Figure 5-2** indicate the sensor electrolyte microstructure differed for each sensor type. To determine the impact of the electrolyte microstructure on water cross-sensitivity, impedance measurements of sensors composed of coarse PSZ particles were collected. The impedance data indicated the electrochemical response for the sensors containing the course PSZ

electrolyte particles did not significantly change when humidified gases were present, as shown if **Figure 5-3**d. Since similar behavior was observed for sensors composed of smaller PSZ particles, it is unlikely that the microstructure of the electrolyte influenced the NO_x sensor response during humidified gas conditions.

5.5   Equivalent Circuit Analysis

To interpret the electrochemical response of the sensors further, equivalent circuit analysis was carried out. The impedance arcs in **Figure 5-3** were simulated using an equivalent circuit model consisting of resistors, R_1 and R_2, and constant phase elements, CPE_1 and CPE_2. **Figure 5-4** shows the equivalent circuit model that was used to analyze the impedance data for each of the sensors in greater depth. The components R_1 and CPE_1 described the resistance and non-ideal capacitance behavior of the electrolyte. Components R_2 and CPE_2 corresponded to the interfacial resistance and non-ideal capacitance behavior at the electrodes. The constants n_1 and n_2 describe the deviation from ideal capacitance behavior.
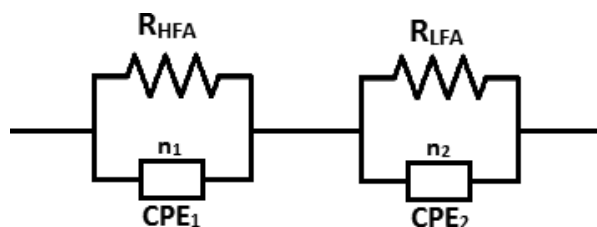
Figure 5-4: Equivalent circuit used to model the impedance data for PSZ, FSZ and composite PSZ–FSZ based sensors.

The behavior of R_2 and CPE_2 are useful for gaining insight about electrode reactions that influence sensing behavior. It was found that the interfacial resistance, R_2, decreased as the operating temperature of the sensor increased. This was expected as interfacial reactions, such as charge transfer, are able to proceed more readily at higher temperatures. The relationship between the capacitance, C, and constant phase element CPE_2 is described by the following equation:

$$C = \frac{[(R_2)(CPE_2)]^{1/n}}{R_2} \pi r^2 \qquad \textbf{Eq. 5-1}$$

where n = 1 describes the behavior of an ideal capacitor. Studies have reported that oxygen coverage at the electrode/electrolyte interface is described by the low frequency arc capacitance [20]. Oxygen accumulation at the electrode/electrolyte interface can hinder NOx transport to the interface and subsequently limit NO_x sensing reactions. **Figure 5-5** shows the capacitance associated with sensors composed of PSZ, FSZ, and 50 PSZ–50 FSZ for dry and humidified gas conditions. The capacitance for sensors with a PSZ electrolyte tended to be an order of magnitude greater than the capacitance of FSZ electrolyte sensors. It is possible that the difference in grain size between the PSZ and FSZ particles contributed to this difference in capacitance [47]. The capacitance of the 50 PSZ–50 FSZ composite electrolyte sensors was about half of the capacitance calculated for the PSZ-based sensors. Adding 3% water to the gas stream caused a slight increase in the capacitance for the PSZ-based sensors, whereas a decrease in the capacitance occurred for FSZ electrolyte sensors and especially the 50 PSZ–50 FSZ-based sensors. Adding additional water did not cause further changes in the capacitance. The addition of NO did not significantly alter the capacitance, which suggests NO molecules did not significantly impact oxygen coverage at the interface.

The data in **Figure 5-5** also indicated a strong temperature dependence for capacitance of the FSZ-based sensors, whereas the PSZ and 50 PSZ–50 FSZ-based sensors displayed a less significant decrease in capacitance as the sensor-operating temperature increased. Overall, it appears the FSZ content in the composite electrolytes was beneficial in limiting oxygen coverage at the interface such that water and NO molecules had greater opportunity to participate in triple-phase-boundary

reactions. The PSZ component of the composite electrolyte helped to limit temperature dependence.
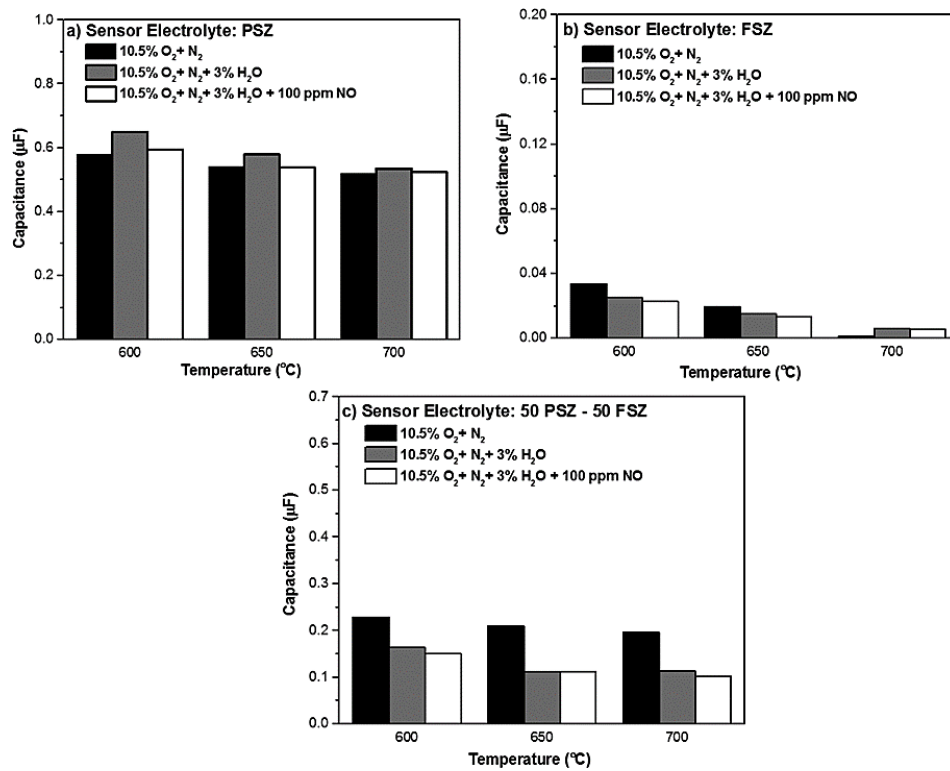
Figure 5-5: The capacitance of (a) PSZ, (b) FSZ and (c) 50 PSZ−50 FSZ based sensors with for dry and humidified gas conditions with respect to temperature.

5.6 Sensor Sensitivity

The angular phase component of the impedance, θ, is often more responsive to the changes in NO_x concentration in comparison to other impedance parameters [19, 48]. For this reason, it is frequently used to evaluate NO_x sensor sensitivity according to **Eq. 2-2**
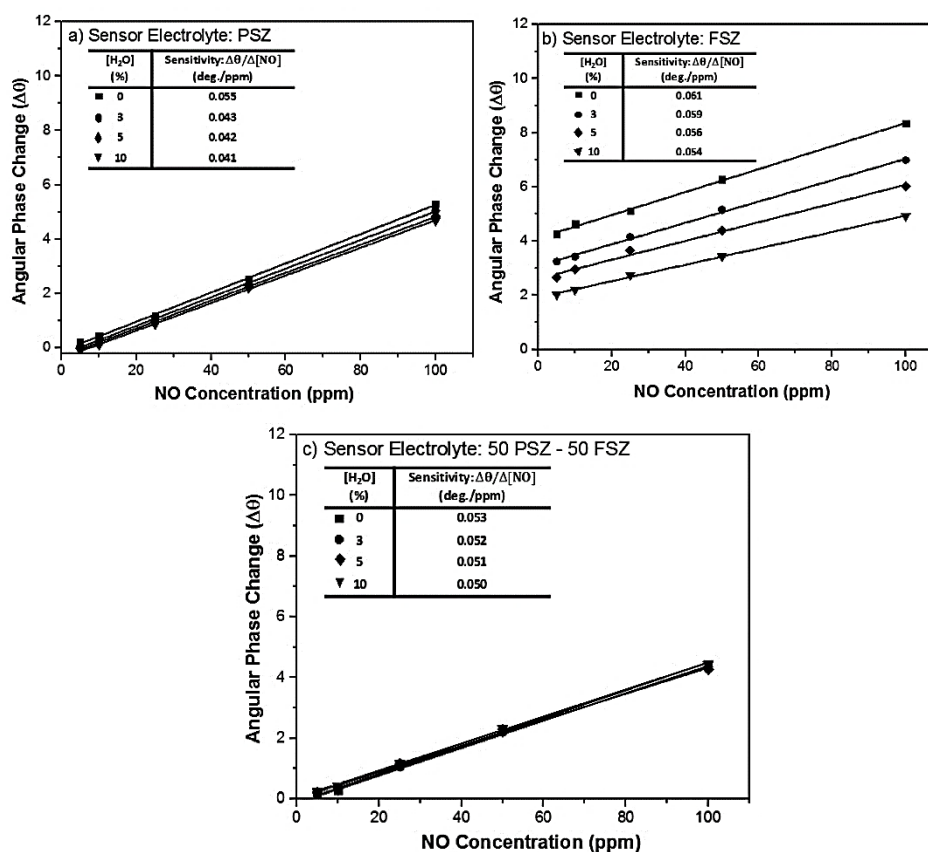
Figure 5-6: NO sensitivity for sensors with: (a) PSZ, (b) FSZ, and (c) 50 PSZ–50 FSZ electrolyte under dry and humidified gas conditions at 650°C.

The change in the angular phase, $\Delta\theta$, is given by **Eq. 4-5**. **Figure 5-6** shows $\Delta\theta$ with respect to NO and water concentration for the PSZ, FSZ, and 50 PSZ–50 FSZ composite-based sensors at an operating frequency of 40 Hz at 650°C. Data was collected at 40 Hz as the maximum sensitivity was achieved at this operating frequency. The slope of the data $\Delta\theta/\Delta[NO]$ is defined as the sensor sensitivity in units of degrees/ppm NO. The highest sensitivity was achieved during dry gas conditions for the various sensors. As the water concentration was increased in the gas stream, the sensitivity of the sensors decreased. However, the 50 PSZ–50 FSZ composite based sensors demonstrated the greatest tolerance to changes in the gas humidity as the sensitivity decreased very slightly.

The sensors with an FSZ electrolyte had a higher sensitivity than sensors composed of PSZ, but the sensitivity of the FSZ based sensors decreased most significantly with increasing water in the gas stream. Although the FSZ electrolyte sensors provide higher sensitivity, the 50 PSZ–50 FSZ electrolyte contributes to a more reliable sensor.
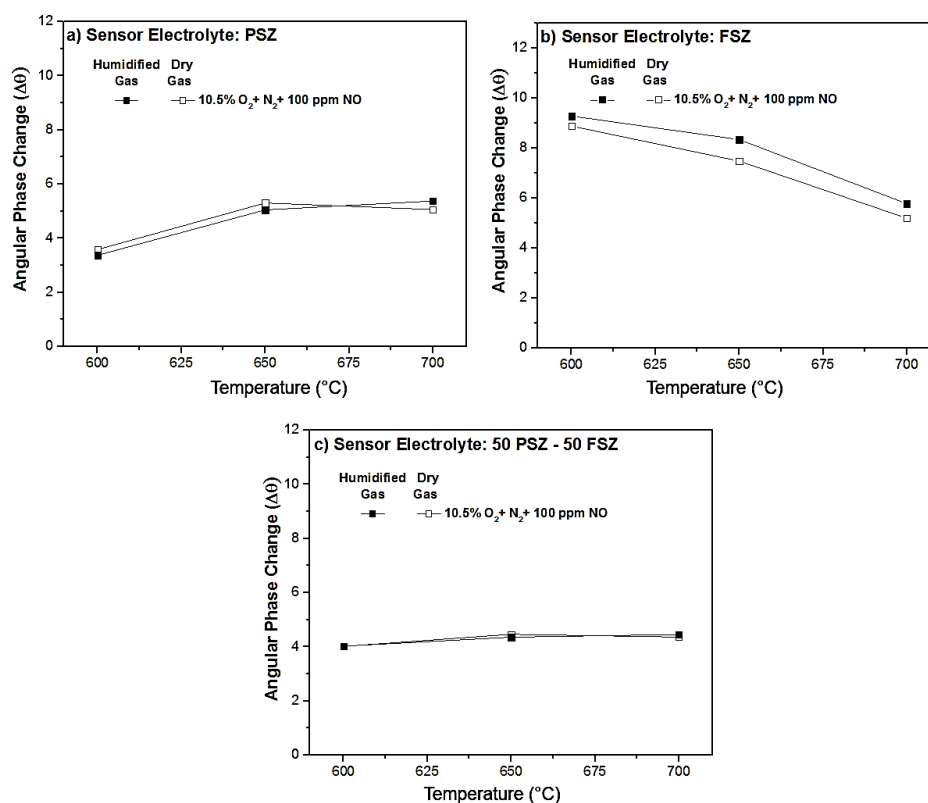
Figure 5-7.Change in angular phase response with respect to temperature for sensors composed of: (a) PSZ, (b) FSZ, and (c) 50 PSZ–50 FSZ electrolyte.

In application, the temperature of the sensor can fluctuate due to changes in driving conditions. Thus, a stable NO_x sensing response with respect to temperature is necessary in order to maintain accuracy. In the present study, the temperature dependence of the various sensors was observed by comparing $\Delta\theta$ with respect to the sensor-operating temperature as shown in **Figure 5-7**.

The sensing response of the FSZ-based sensors decreased with increasing operating temperature as shown in **Figure 5-7**b. However, the PSZ and especially the

50 PSZ–50 FSZ based sensors were less dependent on temperature as shown in
Figure 5-7a and **Figure 5-7**c. This data corresponded with the capacitance data
presented in **Figure 5-5** where the capacitance of the sensors with an FSZ electrolyte
also had a strong temperature dependence in comparison to sensors with a PSZ and
PSZ–FSZ electrolyte. Based on the data shown in **Figure 5-6** and **Figure 5-7**, sensors
with the 50 PSZ–50 FSZ electrolyte were less prone to water cross-sensitivity and
more tolerant to changes in the operating temperature.

5.7   Rate Limiting Mechanisms and Activation Energies

The gases traveling through the porous electrolyte and reacting at the triple-
phase-boundary undergo various reaction steps including adsorption, dissociation,
diffusion, charge transfer, and oxygen ion transport (not necessarily in that order).
The porous microstructure creates specific pathways for gas and ionic transport. The
electrolyte material and microstructure can impact how readily gas transport and
related reactions occur. A common approach to interpreting rate-limiting mechanisms
that impact gas transport and associated reactions is to evaluate the oxygen partial
pressure (P_{O2}) dependence, which is described by the power law relationship as given
in **Eq. 4-6**.

The power law exponent, m, is used to interpret specific rate-limiting
mechanisms, and R_{LFA} is the low frequency arc previously discussed. The P_{O2}
dependence of the PSZ, FSZ, and 50 PSZ–50 FSZ based sensors was determined by
measuring the impedance response at oxygen concentrations ranging from 1 to 18%
for dry and humidified gas conditions with and without NO. A plot of log (R_{LFA})
versus log (P_{O2}) was generated for the various gas conditions in order to determine the
exponent m. **Table 5-2** provides the m values determined for the sensors with a PSZ,
FSZ, and 50 PSZ–50 FSZ electrolyte. Dissociative adsorption is the rate-limiting

mechanism commonly associated with at P_{O2} dependence where $m = 0.5$ [40, 49]. The data in the table indicated under dry gas conditions $m \approx -0.5$ for the PSZ-based sensors, which suggested dissociative adsorption was rate-limiting. Adding water to the gas stream without NO present decreased m to - 0.43 suggesting an additional rate-limiting mechanism, possibly charge transfer, became involved.

Table 5-2: Power law exponent for sensors composed of the various electrolytes.

Power Law Exponent, m				
	NO (ppm)	PSZ	50 PSZ – 50 FSZ	FSZ
Dry Gas	0	-0.494	-0.620	-0.412
	100	-0.465	-0.591	-0.413
Humidified Gas	0	-0.427	-0.626	-0.471
	100	-0.512	-0.553	-0.472

The charge transfer becomes a dominant rate-limiting step when

$$(P_{O2})^{-0.25} \propto R_{LFA} \qquad \textbf{Eq. 5-2}$$

In the presence of NO and water, the PSZ-based sensors were apparently limited by dissociative adsorption as a $(P_{O2})^{-0.51}$ dependence was observed. A slightly lower P_{O2} dependence was determined for the FSZ-based sensors. However, in the presence of both water and NO, the dissociative adsorption seemed to be the dominant rate-limiting mechanism for FSZ-based sensors. Sensors with the composite 50 PSZ– 50 FSZ electrolyte had a stronger P_{O2} dependence in comparison to the other sensors evaluated. The exponent m tended to be about -0.6, which suggested gas diffusion, may have participated as an additional rate-limiting mechanism.

A $(P_{O2})^{-1}$ dependence has been associated with gas diffusion limitations. The porosity of the 50 PSZ–50 FSZ sensor was about 47%, which is expected to provide sufficient gas diffusion. However, it is possible that the composite microstructure resulted in tortuous pathways that interfered with gas diffusion. As a result, the dissociative adsorption and gas diffusion could serve as rate-limiting mechanisms for sensors with a composite electrolyte. The activation energy associated with the various sensors also aids interpretation of how readily sensor reactions are able to proceed. The activation energy, E_a, of the sensors for operating temperatures ranging from 600 to 700°C was determined using the Arrhenius equation given below:

$$\ln\left(\frac{1}{R_{LFA}}\right) = \left(\frac{-E_a}{R}\right)\left(\frac{1}{T}\right) + \ln(A_o) \qquad \textbf{Eq. 5-3}$$

where R_{LFA} is the diameter of the low frequency impedance arc, R represents the ideal gas constant, T is temperature, and A_o is the y-intercept.

Table 5-3 shows the activation energy calculated for each sensor type for dry and humidified conditions with and without NO present. The activation energy was the lowest for the single-phase PSZ-based sensors. The addition of water resulted in an increase in activation energy for the PSZ-based sensors and a decrease in the composite and FSZ-based sensors. Adding FSZ to the sensor electrolyte caused the activation energy to increase. This trend was observed for each of the various gas compositions measured and likely relates to the electrolyte microstructure. Other studies have reported that the activation energy in porous electrolyte NO_x sensors tends to increase with increasing electrolyte porosity [34]. **Table 5-1** shows the porosity of the electrolytes increased as the FSZ content in the sensor electrolyte increased. The increase in porosity causes particle contact along the electrode/electrolyte interface to decrease resulting in fewer sites for reactions to take place, thereby resulting in an increase in the activation energy.

Table 5-3: Activation energy values for the various sensors.

Activation Energy (eV)						
	NO (PPM)	PSZ	75 PSZ – 25 FSZ	50 PSZ – 50 FSZ	25 PSZ – 75 FSZ	FSZ
Dry Gas	0	1.067	1.119	1.148	1.150	1.230
	100	1.017	1.101	1.122	1.125	1.205
Humidified Gas	0	1.084	1.110	1.122	1.133	1.135
	100	1.035	1.043	1.099	1.081	1.082

5.8 Sensor Response Time and Stability

Time-based measurements for the angular phase response, θ, were collected for sensors with a PSZ, FSZ, and composite PSZ–FSZ electrolyte. **Figure 5-8** shows the typical time-based response for sensors with a 50 PSZ–50 FSZ electrolyte as the NO composition was varied over 0–100 ppm. The dry and humidified data overlap as the 50 PSZ–50 FSZ electrolyte enables the sensor to be less prone to water cross-sensitivity. A baseline shift was observed for the time-based data collected for sensors composed the other electrolytes studied. The response time for each sensor was evaluated based on the τ_{90} response, which is the time required for the sensor to achieve 90% of the steady-state response after a step change in gas concentration.
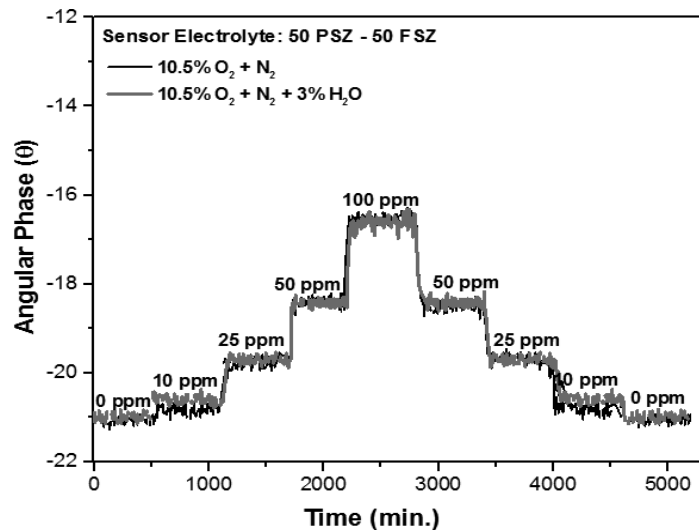
Figure 5-8: Angular phase response with respect to time for sensors composed of a 50 PSZ–50 FSZ electrolyte.

Table 5-4: The τ_{90} response of the sensors composed of the various electrolytes.

Time constant - τ_{90} (sec)					
Sensor Electrolyte	**PSZ**	**75 PSZ – 25 FSZ**	**50 PSZ – 50 FSZ**	**25 PSZ – 75 FSZ**	**FSZ**
Dry Gas	16	14	10	7	5
Humidified Gas	14	12	11	5	4

Table 5-4 shows the τ_{90} response for the various sensors. The sensors

containing single-phase PSZ were the slowest as τ_{90} = 16 s, which possibly relates to

the lower ionic conductivity of the electrolyte, in comparison to single-phase FSZ-

based sensors where τ_{90} = 5s. As seen in **Table 5-4**, the sensor response time

decreased resulting in a faster sensor as the FSZ concentration increased. The stability

of a 50 PSZ–50 FSZ based sensors was evaluated for over 150 hours at 650°C and an

operating frequency of 40 Hz with 3% water present. **Figure 5-9** shows sensor drift

was negligible for both the baseline response where θ remained about -17.25°, and the

sensor response with humidified gas where θ remained nearly constant at about

-16.25°. This data suggests that the 50 PSZ–50 FSZ electrolyte is capable of

providing a very stable sensing response. Further evaluation is necessary to determine

the extent of the 50 PSZ–50 FSZ based sensor stability over longer time intervals.
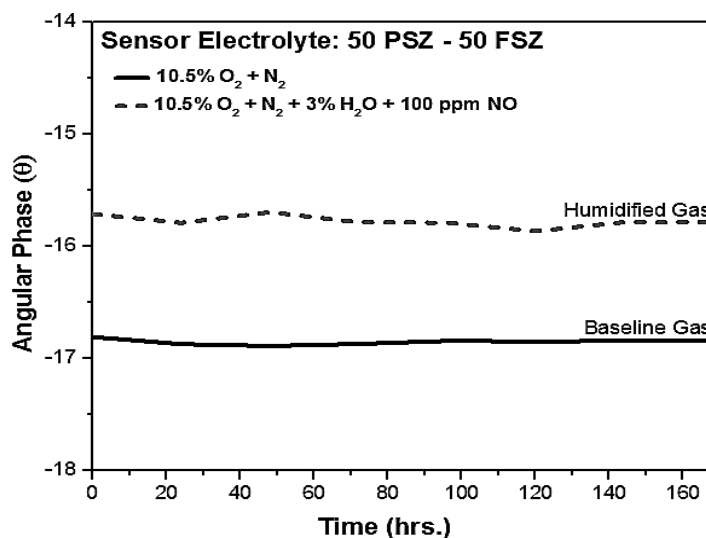
Figure 5-9: Stability of a 50 PSZ–50 FSZ sensor over several hours of operation.

5.9   Conclusions

Impedance spectroscopy was used to interpret the electrochemical response of

NO_x sensors composed of PSZ, FSZ, and PSZ–FSZ composite electrolytes during

operation under dry and humidified gas conditions. Analysis of the electrochemical

response of the 50 PSZ–50 FSZ based sensors indicated PSZ contributed to lower

water cross-sensitivity, while FSZ promoted NO_x sensitivity. It was also determined

that the electrolyte microstructure influenced sensor sensitivity, but did not impact

water cross-sensitivity. Dissociative adsorption was considered to be the dominant

rate-limiting mechanism for each of the sensors. Adding water to the gas stream did

not appear to significantly alter the rate-limiting mechanism. The response of the

FSZ-based sensors was strongly depended upon the operating temperature, whereas

the response of sensors containing PSZ, and particularly the 50 PSZ–50 FSZ, was less

dependent on temperature. The response time of the sensors decreased as the

concentration of FSZ increased within the sensor electrolyte indicating the FSZ

contributed to a rapid sensor response rate. Overall, sensors composed of the 50 PSZ–

50 FSZ composite electrolyte demonstrated significant sensitivity to NO and low

cross-sensitivity to water with negligible temperature dependence.

CHAPTER 6.

ENHANCED COMPOSITE ELECTROLYTES

6.1   Introduction

Based on the results of the studies discussed in Chapters 4 and 5 on PSZ-2%
Al_2O_3 and PSZ-FSZ electrolytes, a composite electrolyte composed of PSZ-FSZ-
2%Al_2O_3 was fabricated in order to capture the beneficial properties of both types of
electrolytes. As demonstrated previously, the PSZ aided the mechanical strength of
the sensor, while the Al_2O_3 increased NO_x sensitivity and further increased
mechanical durability [48]; and the addition of FSZ was expected to minimize water
cross-sensitivity [49]. This work is novel as there are limited studies on the role of
composite porous electrolytes for NO_x sensing. The work presented in the following
section evaluates the sensing characteristics of sensors supported by PSZ-FSZ-2%
Al_2O_3 electrolytes. In addition to the impedance behavior and sinsitivity to NO_x, the
cross-sensitivity to H_2O, O_2, CO, CO_2, and CH_4 are presented. The experiments in this
study along with the fabrication methods were carried out on the standard testing
stand which is the same as the previous chapters.

6.2   Sensor Diagram

A schematic presentation of the top view and cross section of the sensor is
given in **Figure 6-1**. Both top and cross-sectional views illustrate the spacing and
placement of gold electrodes along with the dimensions of electrolyte pellet.
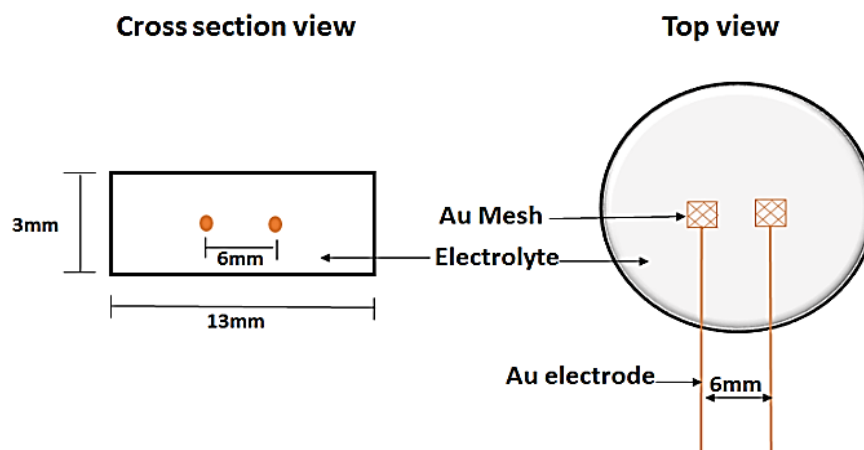
Figure 6-1: Schematic presentation (top and cross-sectional) of a sensor.

6.3   Microstructure and Morphology

Typical surface images of the sensors were collected using SEM are shown in

Figure 6-2. The micrograph was taken using secondary electrons at an accelerating

voltage of 1.0 kV. The electrolyte consisted of well-dispersed particles with varying

dimensions. The fine FSZ particles were about 0.04 µm in diameter, whereas the PSZ

and Al_2O_3 particles were coarse with irregular shapes ranging from 0.4 – 1 µm.

Identification of the various particles was based on microstructural analysis of sensors

composed single phase FSZ and PSZ porous electrolytes, and X-ray diffraction analysis

reported by the authors in prior studies [44, 50]. The electrolyte porosity was measured

by using Archimedes method and it indicated a value of 45 ± % 0.5. Cross-sectional

images porous microstructure was very similar to the surface images.

The sensing electrodes studied were dense Au attached with Au mesh to enhance

current collections. The Au sensing electrode was a wire that was 0.2 mm in diameter.

As shown in Figure 6.1, the Au wire sensing electrode was embedded within the

sensor electrolyte. Prior studies found sensors fabricated with Au wire electrodes with

a greater diameter caused micro-cracks to form within the electrolyte, thereby

compromising the NO$_x$ sensing response. Thus, the 0.2 mm diameter Au wire was used in order to avoid micro-cracks.
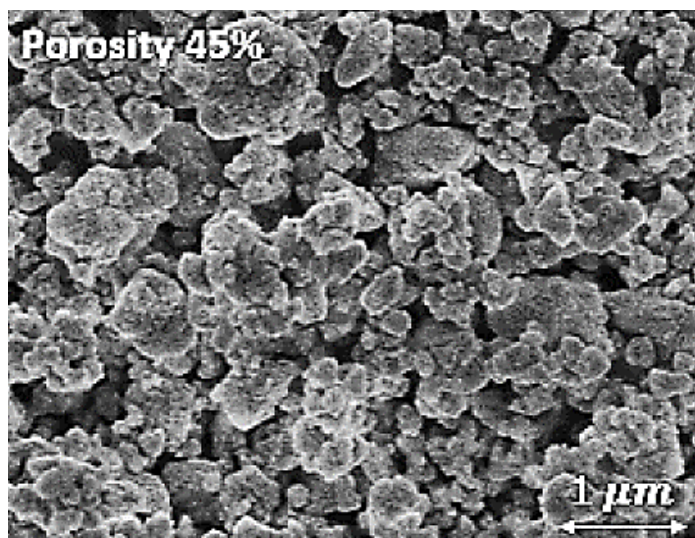

Figure 6-2: Micrograph of the fractured PSZ–FSZ–2% Al$_2$O$_3$ electrolyte.

6.4   Electrochemical Response of NOx Sensors

A typical Nyquist plot showing the electrochemical response of PSZ–FSZ–2% Al$_2$O$_3$ based NO$_x$ sensor is shown in **Figure 6-3**. Impedance spectroscopy measurements taken for assessing the sensor's response to the environment consisting of dry condition with and without NO gas present during operating temperatures 650°C. In case of low frequency arc, a decrease in its magnitude was observed upon addition of the two species, i.e. the base line which represents when the 10.5% O$_2$ and N$_2$ is balanced and 100 ppm NO in the dry environment. This signified a fact that the reactions at electrode and electrolyte interface occur more readily in the presence of the above-mentioned species. Apparently, NO causes change in the conductance of FSZ–PSZ–2% Al$_2$O$_3$/Au sensor [22]. The work represented here is focused on the behavior of the sensors in the presence of NO gases since the sensors, response operate with NO$_2$ was equivalent to that for NO because of the thermodynamic conversion at higher temperatures.
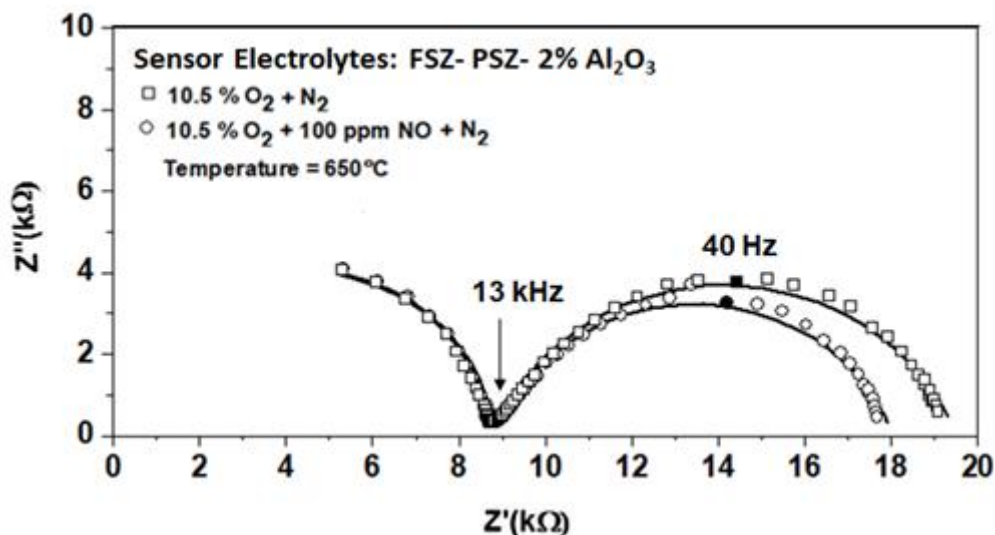
Figure 6-3: Impedance response of the FSZ–PSZ–2% Al_2O_3 based sensor.

6.5 NO Sensitivity

Phase angle, defined as the ratio of capacitive and resistive components, is considered as more responsive to change in concentration of any gas [51]. As shown in **Figure 6-4**, the phase angle measurements were carried out for the three different electrolytes in the presence of 650°C and NO concentration ranging from 0-100 ppm. The largest $\Delta\theta$ values occurred at 40 Hz for the electrolyte based sensors. PSZ–FSZ–2% Al_2O_3 composite electrolyte sensors demonstrate superior sensitivity to NO_x in comparison to PSZ-2% Al_2O_3 and PSZ-FSZ based sensors. The enhancement of the sensitivity of the PSZ–FSZ–2% Al_2O_3 composite electrolyte is likely due to the higher ionic conductivity of the FSZ electrolyte, in comparision to PSZ, along with the contribution of the Al_2O_3 particles to enhance conductivity along PSZ grain boundaries that enabled electrochemical reactions involving oxygen ions and NO to proceed more readily.
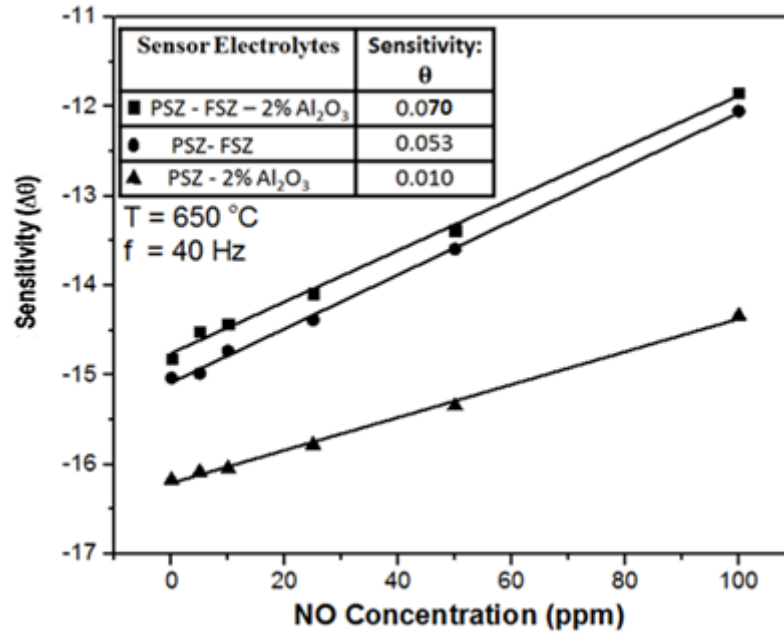
Figure 6-4: NO_x sensitivity for FSZ–PSZ–2% Al_2O_3.

6.6 Cross-sensitivity to H_2O, O_2, CO, CO_2, and CH_4

6.6.1 Water Cross-sensitivity

In **Figure 6-5**, the Nyquist plots for dry and 3% humidified conditions have been shown for FSZ-PSZ–2% Al_2O_3 in the presence of 100 ppm NO at 650°C. The performance significantly changes with the addition of water. This indicated that the presence of Al_2O_3 did not impact water reactions, and that water did not interfere with NO_x sensitivity at the PSZ-FSZ-2%Al_2O_3 based sensors.
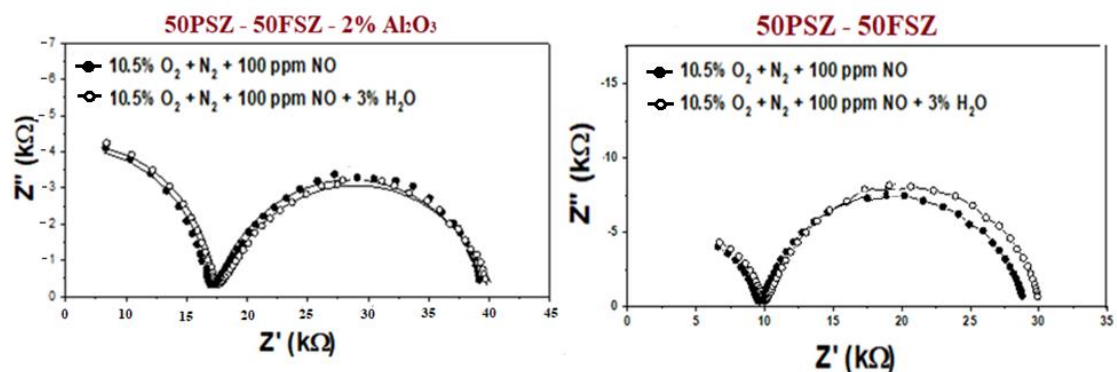
Figure 6-5: Impedance response for (a) PSZ-FSZ –2% Al_2O_3 (b) PSZ-FSZ sensors with and without 3% H_2O.

6.6.2　　　Cross-sensitivity CO, CO$_2$, and CH$_4$

Figure 6-6 demonstrates the sensing behavior according to the phase angle for PSZ-FSZ-2%Al$_2$O$_3$ based sensors operating with 100 ppm CO, CO$_2$ and CH$_4$ over time. Although the response appeared to be rapid and stable, the PSZ–FSZ–2% Al$_2$O$_3$ based sensors showed substantial cross-sensitivity to all three different gases. This suggests that the composite electrolyte is not selective to NO$_x$, and therefore, it is not feasible for NO$_x$ sensing. However, analysis of the frequency response for NO and CH$_4$, shown in **Figure 6-7**, indicates the peak phase response occurred at different frequencies. This indicates the NO response could be monitored by operating the sensor at 100 Hz. This data also suggests there is potential for measuring different gases at different frequencies. For example, based on the different peak phase responses for NO and CH$_4$, it could be possible to operate the sensor at 100 Hz for NO detection and at 400 Hz to detect CH$_4$. If further studies that verify different frequencies can be distinguished for other gases, then it could be possible to operate a PSZ-FSZ-2%Al$_2$O$_3$ type sensor as a multi-gas sensor. This idea is highly attractive as the current methods for multi-gas sensors rely on multiple columns or sensing arrays that add to the bulk and complexity of the device.
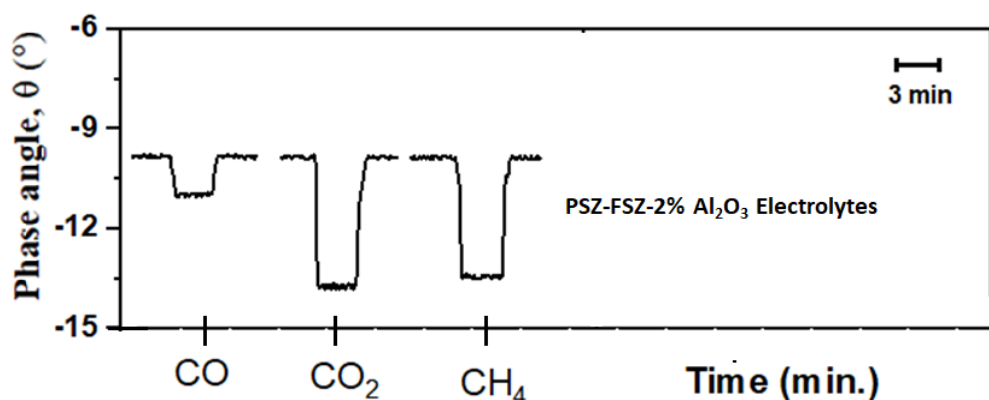
Figure 6-6: Selectivity study for PSZ–FSZ–2% Al$_2$O$_3$ (650ºC, 40 Hz) sensors using air as the base gas.
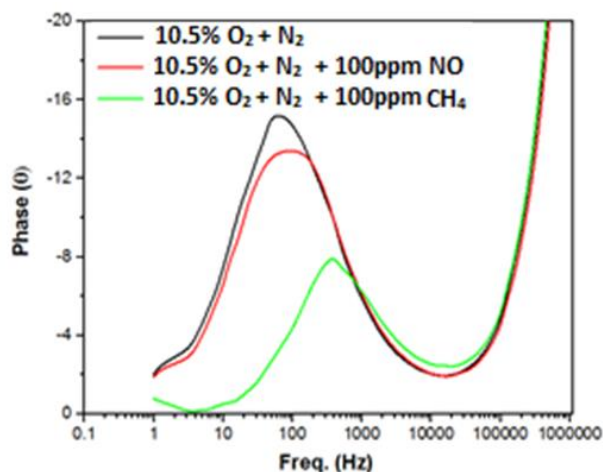
Figure 6-7: Phase response of PSZ–FSZ–2% Al_2O_3-sensor with 100 ppm NO and CH_4 present.

6.7   Long-term Functionality

Sensors were further tested for its long-term functionality as shown in **Figure 6-88** under low noise phase response conditions, i.e. temperature of 650°C and frequency of 40 Hz. Any change in phase angle shift (θ) or sensor's sensitivity was studied for 30 days under 100 ppm NO balanced with 10.5% O_2 and N_2. It was found that only the presence of NO caused a shift in θ output as compared to the baseline gas. Throughout the testing period, the θ output stayed constant showing a stable sensor response. Such behavior of the sensor is beneficial for its practical applications [52].
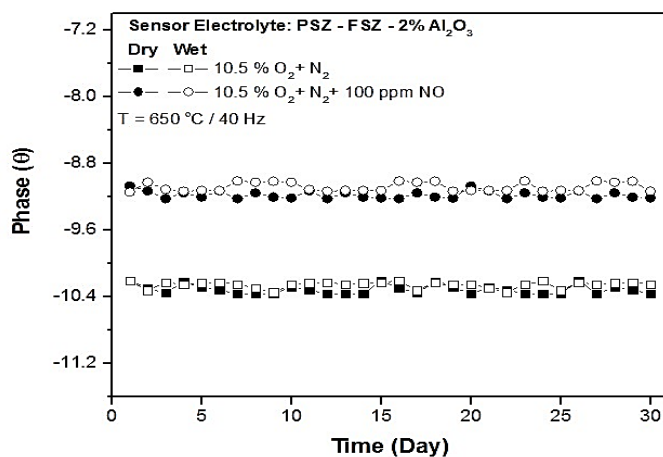
Figure 6-8: Phase angle shift response for PSZ–FSZ–2% Al_2O_3 sensor over several days of operation.

6.8   Conclusions

In this research study, PSZ-FSZ-2%Al_2O_3 composite electrolytes were investigated in terms of NO sensitivity, cross-sensitivity to H_2O, O_2, CO,CO_2, and CH_4 and long-term stability. The sensitivity of the composite PSZ-FSZ-2%Al_2O_3 sensors showed superior NO sensitivity as well as lower water cross-sensitivity compared with the previous study in Chapters 4 and 5, respectively. Cross-sensitivity to CO, CO_2, and CH_4 was observed; however, it is possible that this can be addressed by operating the sensor at different frequencies in order to distinguish the response to different gases. Such operation would enable multi-gas sensing. The time-based data collected over 30 days indicated the PSZ-FSZ-2%Al_2O_3 based sensors were very stable.

CHAPTER 7.

CONCLUSIONS AND FUTURE WORK

Some of the important conclusions that can be drawn from this research study are listed as follows:

- The addition of Al2O3 to PSZ in various concentrations (2, 3.8, 5 and 10 wt.%) resulted in an increase in the NO sensor impedance. The addition of 2 wt% Al2O3 enhanced the PSZ electrolyte grain boundary conductivity. However, increasing the Al2O3 addition above 2 wt.% in the PSZ electrolyte increased the resistance of the electrolyte bulk, grain boundaries and interfacial reactions. Overall, the addition of 2 wt.% Al2O3 to PSZ based sensors resulted in greater sensitivity to NOx, and sensitivity was achieved at concentrations as low as 5 ppm.

- Composite electrolytes were also studied by using impedance spectroscopy for the electrochemical response, gas sensitivity, rate limiting mechanisms, and sensing response rate in humidified gas environments. The tested NOx sensors were composed of PSZ, FSZ, and PSZ-FSZ composite electrolytes which were operated under dry and humidified gas conditions. The response of 50 PSZ-50 FSZ based sensors indicated PSZ contributed to lower water cross-sensitivity, while FSZ promoted NOx sensitivity. It was also found that the electrolyte microstructure influenced the sensor's sensitivity, but did not impact water cross-sensitivity. The FSZ-based sensors exhibited a rapid sensor response rate which was strongly dependent upon the operating temperature, whereas the response of sensors

containing PSZ, and particularly the 50 PSZ-50 FSZ, was less dependent on temperature.

BIBLIOGRAPHY

[1]   R. P. Ltd. (2017). *What diesel vehicle owners need to know*. Available: https://www.rix.co.uk/errors/404.aspx?aspxerrorpath=/blog/2016/7/adblue-what-diesel-vehicle-owners-need-to-know/

[2]   J. Meulenbelt, "Nitrogen and Nitrogen Oxides," *Medicine,* vol. 31, no. 10, p. 64, 2003.

[3]   V. Vestreng, L. Ntziachristos, A. Semb, S. Reis, I. S. Isaksen, and L. Tarrasón, "Evolution of NO x emissions in Europe with focus on road transport control measures," *Atmospheric Chemistry and Physics,* vol. 9, no. 4, pp. 1503-1520, 2009.

[4]   G. L. Borman and K. W. Ragland, *Combustion engineering*. McGraw-Hill Science/Engineering/Math, 1998.

[5]   DieselNet. (2017, 12th September). *DieselNet Technology Guide*. Available: https://www.dieselnet.com/standards/cn/hd.php

[6]   E. M. Logothetis and R. E. Soltis, "Method for determining relative amount of oxygen containing gas in a gas mixture," ed: Google Patents, 1992.

[7]   J. W. Fergus, "Materials for high temperature electrochemical NO x gas sensors," *Sensors and Actuators B: Chemical,* vol. 121, no. 2, pp. 652-663, 2007.

[8]   N. Kato, H. Kurachi, and Y. Hamada, "Thick film ZrO2 NOx sensor for the measurement of low NOx concentration," SAE Technical Paper0148-7191, 1998.

[9]   "Bringing the world's first high-precision NOx sensor to market," ed: NGK Insulators, Ltd., 2008.

[10]   T. Ono, M. Hasei, A. Kunimoto, T. Yamamoto, and A. Noda, "Performance of the NO x sensor based on mixed potential for automobiles in exhaust gases," *JSAE review,* vol. 22, no. 1, pp. 49-55, 2001.

[11]   N. Miura, G. Lu, and N. Yamazoe, "High-temperature potentiometric/amperometric NO x sensors combining stabilized zirconia with mixed-metal oxide electrode," *Sensors and Actuators B: Chemical,* vol. 52, no. 1, pp. 169-178, 1998.

[12]   T. Striker, V. Ramaswamy, E. N. Armstrong, P. D. Willson, E. D. Wachsman, and J. A. Ruud, "Effect of nanocomposite Au–YSZ electrodes on potentiometric sensor response to NO x and CO," *Sensors and Actuators B: Chemical,* vol. 181, pp. 312-318, 2013.

[13]   H. L. Tuller, "Materials for high temperature electrochemical applications: automotive sensors, catalysts and traps," *Sensors and Actuators B: Chemical,* vol. 187, pp. 106-110, 2013.

[14]   S. Zhuiykov, *Electrochemistry of zirconia gas sensors*. CRC Press, 2007.

[15]   J. M. Rheaume, *Solid State Electrochemical Sensors for Nitrogen Oxide (NOx) Detection in Lean Exhaust Gases*. University of California, Berkeley, 2010.

[16]   DieselNet. (2017, 9th May). *Cars and Light-Duty Trucks—Tier 3*. Available: https://www.dieselnet.com/standards/us/ld_t3.php#ftp

[17]   R. Cottis and S. Turgoose, "Electrochemical impedance and noise," 1999.

[18]   R. Barfod, A. Hagen, S. Ramousse, P. Hendriksen, and M. Mogensen, "Break down of losses in thin electrolyte SOFCs," *Fuel Cells,* vol. 6, no. 2, pp. 141-145, 2006.

[19]   L. P. Martin, L. Y. Woo, and R. S. Glass, "Impedancemetric NO x Sensing Using YSZ Electrolyte and YSZ∕Cr2O3 Composite Electrodes," *Journal of The Electrochemical Society,* vol. 154, no. 3, pp. J97-J104, 2007.

[20]   L. Y. Woo *et al.*, "Effect of electrode composition and microstructure on impedancemetric nitric oxide sensors based on YSZ electrolyte," *Journal of the Electrochemical Society,* vol. 155, no. 1, pp. J32-J40, 2008.

[21]   L. Y. Woo, R. S. Glass, R. F. Novak, and J. H. Visser, "Effect of electrode material and design on sensitivity and selectivity for high temperature impedancemetric NO x sensors," *Journal of The Electrochemical Society,* vol. 157, no. 3, pp. J81-J87, 2010.

[22]   J. M. Rheaume and A. P. Pisano, "A review of recent progress in sensing of gas concentration by impedance change," *Ionics,* vol. 17, no. 2, pp. 99-108, 2011.

[23]   S. Killa, L. Cui, E. P. Murray, and D. S. Mainardi, "Kinetics of nitric oxide and oxygen gases on porous Y-stabilized ZrO2-based sensors," *Molecules,* vol. 18, no. 8, pp. 9901-9918, 2013.

[24]   R. Mukundan, K. Teranishi, E. L. Brosha, and F. H. Garzon, "Nitrogen oxide sensors based on yttria-stabilized zirconia electrolyte and oxide electrodes," *Electrochemical and solid-state letters,* vol. 10, no. 2, pp. J26-J29, 2007.

[25]   F. H. Garzon, R. Mukundan, R. Lujan, and E. Brosha, "Solid state ionic devices for combustion gas sensing," *Solid State Ionics,* vol. 175, no. 1, pp. 487-490, 2004.

[26]   M. Borik *et al.*, "Phase composition, structure and mechanical properties of PSZ (partially stabilized zirconia) crystals as a function of stabilizing impurity content," *Journal of Alloys and Compounds,* vol. 586, pp. S231-S235, 2014.

[27]   S. Celik, B. Timurkutluk, S. Toros, and C. Timurkutluk, "Mechanical and electrochemical behavior of novel electrolytes based on partially stabilized zirconia for solid oxide fuel cells," *Ceramics International,* vol. 41, no. 7, pp. 8785-8790, 2015.

[28]   E. Drożdż, M. Jelonek, J. Wyrwa, and M. Rękas, "The Influence Of The Way Of Alumina Addition On Properties Improvement Of 3YSZ Material," *Archives of Metallurgy and Materials,* vol. 60, no. 2, pp. 999-1002, 2015.

[29]   C. Zhang *et al.*, "Ionic conductivity and its temperature dependence of atmospheric plasma-sprayed yttria stabilized zirconia electrolyte," *Materials Science and Engineering: B,* vol. 137, no. 1, pp. 24-30, 2007.

[30]   A. Feighery and J. Irvine, "Effect of alumina additions upon electrical properties of 8 mol.% yttria-stabilised zirconia," *Solid State Ionics,* vol. 121, no. 1, pp. 209-216, 1999.

[31]   J. P. Angle, J. J. Steppan, P. M. Thompson, and M. L. Mecartney, "Parameters influencing thermal shock resistance and ionic conductivity of 8 mol% yttria-stabilized zirconia (8YSZ) with dispersed second phases of alumina or mullite," *Journal of the European Ceramic Society,* vol. 34, no. 16, pp. 4327-4336, 2014.

[32]   M. Abden, M. Islam, and J. Afroze, "Microstructure and Mechanical Properties of 3YSZ Ceramics Rainforced with Al 2 O 3 Particles," *International Journal of Materials Engineering,* vol. 4, no. 4, pp. 129-135, 2014.

[33]   S. J. Glass and D. J. Green, "Mechanical Properties of Infiltrated Alumina-Y-TZP Composites," *Journal of the American Ceramic Society,* vol. 79, no. 9, pp. 2227-2236, 1996.

[34]   L. Cui, F. Han, W. Dai, and E. P. Murray, "Influence of microstructure on the sensing behavior of NOx exhaust gas sensors," *Journal of The Electrochemical Society,* vol. 161, no. 3, pp. B34-B38, 2014.

[35]   M. Bengisu, *Engineering ceramics*. Springer Science & Business Media, 2013.

[36]   J. Macdonald and W. Johnson, "Impedance Spectroscopy: Theory, Experiments, and Applications, edited by E. Barouskov and JR Macdonald," ed: Wiley-VCH, New York, 2005.

[37]   M. Steil, F. Thevenot, and M. Kleitz, "Densification of Yttria-Stabilized Zirconia Impedance Spectroscopy Analysis," *Journal of the Electrochemical Society,* vol. 144, no. 1, pp. 390-398, 1997.

[38]   S. P. S. Badwal, "Effect of dopant concentration on the grain boundary and volume resistivity of yttria-zirconia," *Journal of materials science letters,* vol. 6, no. 12, pp. 1419-1421, 1987.

[39]   J. v. Herle, A. McEvoy, and K. R. Thampi, "Conductivity measurements of various yttria-stabilized zirconia samples," *Journal of materials science,* vol. 29, no. 14, pp. 3691-3701, 1994.

[40]   S. Raz, K. Sasaki, J. Maier, and I. Riess, "Characterization of adsorbed water layers on Y 2 O 3-doped ZrO 2," *Solid State Ionics,* vol. 143, no. 2, pp. 181-204, 2001.

[41]   L. Woo, R. Glass, R. Novak, and J. Visser, "Diesel engine dynamometer testing of impedancemetric NO x sensors," *Sensors and Actuators B: Chemical,* vol. 157, no. 1, pp. 115-121, 2011.

[42]   R. Soltis, Y. Ding, D. J. Kubinski, and J. H. Visser, "Influence of H2O on NOx Sensors," *ECS Transactions,* vol. 3, no. 10, pp. 173-178, 2006.

[43]   N. Sakai *et al.*, "Erratum to "Effect of water on electrochemical oxygen reduction at the interface between fluorite-type oxide-ion conductors and various types of electrodes"," *Solid State Ionics,* vol. 176, no. 29, pp. 2327-2333, 2005.

[44]   K. Kharashi and E. P. Murray, "Effect of Al2O3 in Porous Zirconia Electrolytes for NO Sensing," *Journal of The Electrochemical Society,* vol. 163, no. 13, pp. B633-B637, 2016.

[45]   Y. Kuroda, H. Hamano, T. Mori, Y. Yoshikawa, and M. Nagao, "Specific adsorption behavior of water on a Y2O3 surface," *Langmuir,* vol. 16, no. 17, pp. 6937-6947, 2000.

[46]   D. T. Chaopradith, D. O. Scanlon, and C. R. A. Catlow, "Adsorption of water on yttria-stabilized zirconia," *The Journal of Physical Chemistry C,* vol. 119, no. 39, pp. 22526-22533, 2015.

[47]   X. Guo and J. Maier, "Grain boundary blocking effect in zirconia: a Schottky barrier analysis," *Journal of the Electrochemical Society,* vol. 148, no. 3, pp. E121-E126, 2001.

[48]   K. Indira and T. Nishimura, "In-Situ Electrochemical Monitoring and Ex-Situ Chemical Analysis of Epoxy Coated Steels in Sodium Chloride Environment Using Various Spectroscopic Techniques," *Transactions of the Indian Institute of Metals,* pp. 1-14, 2017.

[49]   A. McEvoy and K. R. Thampi, "Oxygen reduction at porous and dense cathodes for solid oxide fuel cells," *Electrochimica acta,* vol. 39, no. 11-12, pp. 1675-1680, 1994.

[50]   E. P. Murray, K. Kharashi, and K. Adedeji, "Managing H2O Cross-Sensitivity Using Composite Electrolyte NOx Sensors," in *Electrochemical Sensors Technology*: InTech, 2017.

[51]   L. Y. Woo, R. Glass, R. Novak, and J. Visser, "Impedancemetric NOx Sensing Based On Porous Yttria-Stabilized Zirconia (YSZ) Electrolyte: Effect of Electrode Materials on Total-NOx Sensing and Stability," in *Meeting Abstracts*, 2009, no. 45, pp. 1503-1503: The Electrochemical Society.

[52]   V. Franco, F. P. Sánchez, J. German, and P. Mock, "Real-world exhaust emissions from modern diesel cars," *communications,* vol. 49, no. 30, pp. 847129-102, 2014.